PNAS
www.pnas.org

Supplementary Information for

Pericentromeric noncoding RNA changes DNA binding of CTCF and inflammatory gene expression in senescence and cancer

Kenichi Miyata, Yoshinori Imai, Satoshi Hori, Mika Nishio, Tze Mun Loo, Ryo Okada, Liying Yang, Tomoyoshi Nakadai, Reo Maruyama, Risa Fujii, Koji Ueda, Li Jiang, Hao Zheng, Shinya Toyokuni, Toyonori Sakata, Katsuhiko Shirahige, Ryosuke Kojima, Mizuho Nakayama, Masanobu Oshima, Satoshi Nagayama, Hiroyuki Seimiya, Toru Hirota, Hideyuki Saya, Eiji Hara, and *Akiko Takahashi

***Corresponding Author**: Akiko Takahashi, Project for Cellular Senescence, Cancer Institute, Japanese Foundation for Cancer Research, 3-8-31 Ariake, koutou-ku, Tokyo 135-8550, Japan.

Phone: 813-3570-0605; Fax：813-3570-0457; E-mail: akiko.takahashi@jfcr.or.jp

This PDF file includes:

Supplementary Information Methods

Cell Culture

TIG-3 cells (1-3) and IMR-90 cells were obtained from the Japanese Cancer Research Resources Bank and American Type Culture Collection, respectively. TIG-3 cells, IMR-90 cells and IMR-90/ER:H-Ras^{V12} cells (1) were cultured in Dulbecco's Modified Eagle's (DME) medium (Nacalai Tesque) supplemented with 10% fetal bovine serum (FBS) and penicillin/streptomycin (Sigma-Aldrich) at physiological oxygen conditions (92% N_2, 5% CO_2, and 3% O_2) at 37°C. RPE-1/hTERT cells (4) and HEK-293T cells (1) were cultured in DME medium (Nacalai Tesque) supplemented with 10% FBS and penicillin/streptomycin (Sigma-Aldrich) in a 5% CO_2 incubator at 37°C. SVts8 cells (5) were cultured in DME medium (Nacalai Tesque) supplemented with 10% FBS and penicillin/streptomycin (Sigma-Aldrich) in a 5% CO_2 incubator at 34°C. Mouse embryonic fibroblasts (MEFs) were generated from CD-1 mice as previously described (6) and then cultured in DME medium (Nacalai Tesque) supplemented with 10% FBS and penicillin/streptomycin (Sigma-Aldrich) at physiological oxygen conditions (92% N_2, 5% CO_2, and 3% O_2) at 37°C. All cell lines used were negative for mycoplasma.

To induce doxorubicin (DXR)-induced senescence, TIG-3 and RPE-1/hTERT cells were cultured in medium containing DXR at concentrations of 250 and 150 ng/mL, respectively. One day before DXR-treatment, TIG-3 and RPE-1/hTERT cells were plated at a density of 5,000 and 3,637 cells•cm^{-2}, respectively. These cells were not passaged after DXR treatment. To cause X-ray (XRA)-induced senescence, IMR-90, SVts8, and RPE-1/hTERT cells were exposed to 10-, 12-, and 40-gray (Gy) irradiation, respectively, with a CP-160 X-ray machine (Faxitron X-ray Corporation). After XRA irradiation, IMR-90, SVts8, and RPE-1/hTERT cells were plated at a density of 2,500, 9,090 and 4,000 cells•cm^{-2}, respectively. These cells were not passaged for 10 days after XRA irradiation. The induction of oncogene-induced senescence in IMR-90/ER:H-Ras^{V12} cells were performed as previously described (1).

Plasmid Construction

Human centromeric satellite α (hSATα) and pericentromeric satellite II (hSATII) RNAs were cloned from the cDNA derived from DXR-treated RPE-1/hTERT cells and inserted into a pGEM-T Easy Vector (Promega). These cDNAs were tandemly connected in triplet and then subcloned into either a pcDNA3 vector (Invitrogen) or MaRX-puro retrovirus vector (7). Mouse centromeric minor satellite (MinSAT) and pericentromeric major satellite (MajSAT) RNAs were cloned from cDNAs derived from MEFs and inserted into a pGEM-T Easy Vector (Promega). These cDNAs were subsequently subcloned into a pcDNA3 vector (Invitrogen) or MaRX-puro retrovirus vector (7).

The 3xFLAG-tagged CTCF cDNA was cloned into a pcDNA3 vector (Invitrogen), MaRX-puro retrovirus vector (7), or pLenti CMV GFP Puro (658-5) (#17448, Addgene) using an In-Fusion HD Cloning Kit (Clontech) according to the manufacturer's instructions. For the construction to delete all 11 zinc finger (ZF) domains (CTCFΔZF1-11), the following primers were used: 5′-GAAAGGTGTA AAGAAGACAT TCGGCCCAGA TGGCGTAGAG GGGGAAAATG GAGGAG-3′ (Forward) and 5′-CTCCTCCATT TTCCCCCTCT ACGCCATCTG GGCCGAATGT CTTCTTTACA CCTTTC-3′ (Reverse). For the construction of CTCFΔZF1 and CTCFΔZF10, indicating

the deletion of ZF domains 1 and 10, respectively, the primers were used as previously reported (8). For the construction of CTCFΔZF3-6, which spans the deletion of ZF domains 3–6, the following primers were used: 5′-CAGGTACTCG TCCTACAGAA AATGTGGCC-3′ (Forward) and 5′-GGCCACATTT TCTGTAGGAC GAGTACCTG-3′ (Reverse).

All cDNAs were sequenced on a Genetic Analyzer 3130 (Applied Biosystems) using a BigDye Terminator v3.1 Cycle Sequencing Kit (Applied Biosystems).

RNA Interference (RNAi) and Overexpression

The knockdown of CTCF and hSATII RNA were performed by the transfection of small interfering RNAs (siRNAs) using Lipofectamine RNAiMAX Transfection Reagent (Thermo Fisher Scientific), according to the manufacturer's instructions. siRNAs targeting CTCF (Thermo Fisher Scientific, #HSS116455 and #HSS116456) and Negative Control (Duplex High GC Duplex) siRNA (Thermo Fisher Scientific, #46-2000) were used at a concentration of 50 nM for 2 days. Two siRNAs targeting hSATII RNA (#1: 5'-UUUCCAUUCC AUUCCAUUC-3' and #2: 5'-AAUCAUCGAA UGGUCUCGA-3') and one for Negative Control (5'-AUGAACGUGA AUUGCUCAA-3') were used at the concentration of 20 nM for 2 days. As shown in Fig. **1*H***, siRNA #2 targeting hSATII RNA was treated to proliferating or XRA-induced senescent SVts8 cells. Knockdown efficiency was evaluated using real-time quantitative polymerase chain reaction (RT-qPCR).

Retroviral gene transfer into SVts8 cells (*SI Appendix*, Fig. S5) was conducted by transient transfection of LinXE ecotropic packaging cells with a MaRX-puro vector and the vector containing hSATII DNA, as previously described (7). Infected cell populations were selected for 3 days in the presence of 1 μg/mL puromycin. Retroviral gene transfer into early-passage primary MEF cells (P1–P3, *SI Appendix*, Fig. S6) was conducted by transient transfection of LinXE ecotropic packaging cells with a MaRX-puro vector and the vector containing MajSAT DNA, as previously described (6, 7). Infected cell populations were selected for 5 days in the presence of 1 μg/mL puromycin.

SVts8 (**Fig. 2*E***) or HEK-293T (**Fig. 2*C*** and ***D***) cells were transfected with a vector designed to express hSATII RNA and/or CTCF using X-tremeGENE HP DNA Transfection Reagent (Roche), according to the manufacturer's instructions. After 24 hours of transfection, the cells were scraped and analyzed. We monitored the transfection efficiency of CTCF using EGFP expression (the same backbone plasmid with CTCF) and confirmed almost 100% efficiency in each experiment. Although CTCF overexpression generally causes cell cycle arrest, in SVts8 cells in which pRb and p53 are inactivated by large T antigen, we could avoid cell cycle arrest and thereby examined the effect of CTCF overexpression within 24 h. SVts8 cells (**Fig. 1*E*** and ***F*** and **3**; *SI Appendix*, Fig. S2*A*–*C*) were transfected with a vector designed to express hSATII RNA using X-tremeGENE HP DNA Transfection Reagent (Roche) a total of four times every other day, according to the manufacturer's instructions. Cells were scraped and analyzed 24 hours after the final transfection.

Lentiviruses encoding 3xFLAG-tagged CTCF or CTCFΔZF were generated by using Lentiviral Packaging Mix (Sigma-Aldrich, #SHP001) according to the manufacturer's instructions.

Reverse Transcription PCR (RT-PCR)

Total RNA was extracted with TRIzol Reagent (Thermo Fisher Scientific). After removing genomic DNA contamination using a TURBO DNA-*free* Kit (Applied Biosystems), the extracted RNA underwent reverse transcription using a PrimeScript RT Master Mix (TaKaRa). RT-PCR was performed on a Veriti Thermal Cycler (Applied Biosystems) using KOD -Plus- Neo DNA polymerase (Toyobo). The primers used for RT-PCR are as follows: human GAPDH: 5′-GCCACATCGC TCAGACAC-3′ (Forward) and 5′-CATCACGCCA CAGTTTCC-3′ (Reverse); mouse GAPDH: 5′-CAACTACATG GTCTACATGT TC-3′ (Forward) and 5′-CGCCAGTAGA CTCCACGAC-3′ (Reverse); EXOtic-hSATα: 5′-GTTTAAACTT AAGCTCAACG AAGGCCACAA-3′ (Forward) and 5′-CTATTTTGCA TCTAGAAGGT CAATGGCAGA-3′ (Reverse); EXOtic-hSATII: 5′-GCAGTACATC AATGGGCGTGG-3′ (Forward) and 5′-CGCCCATTCG ATGATTGGAT CC-3′ (Reverse); EXOtic Control (Backbone): 5′-GACTTTAGAG GGTACCGTGA TCCG-3′ (Forward) and 5′-GCTGGCAACT AGAAGGCACA G-3′ (Reverse). The amplification products were separated using 1%–3% agarose gel electrophoresis and detected by ethidium bromide staining.

RT-qPCR

Total RNA was extracted with TRIzol Reagent (Thermo Fisher Scientific). After removing genomic DNA contamination using a TURBO DNA-*free* Kit (Applied Biosystems), the extracted RNA underwent reverse transcription using a PrimeScript RT Master Mix (TaKaRa). RT-qPCR was performed on a StepOne Plus PCR system (Thermo Fisher Scientific) using SYBR *Premix Ex Taq* II (Tli RNaseH Plus, TaKaRa, #RR820A). The primers used for RT-qPCR are as follows: hSATII: 5′-AATCATCGAA TGGTCTCGAT-3′ (Forward) and 5′-ATAATTCCAT TCGATTCCAC-3′ (Reverse); hSATα: 5′-AAGGTCAATG GCAGAAAAGAA-3′ (Forward) and 5′-CAACGAAGGC CACAAGATGTC-3' (Reverse); human ACTB: 5'-AGAGCTACGA GCTGCCTGAC-3' (Forward) and 5'-AGCACTGTGT TGGCGTACAG-3' (Reverse); MajSAT: 5′-ATAATTCCAT TCGATTCCAC-3′ (Forward) and 5′-CTTGCCATAT TCCACGTCCT-3′ (Reverse); MinSAT: 5′-TTGGAAACGG GATTTGTAGA-3′ (Forward) and 5′-CGGTTTCCAA CATATGTGTTTT-3′ (Reverse); murine ACTB: 5'-CGCCACCAGT TCGCCATGGA-3' (Forward) and 5'-TACAGCCCGG GGAGCATCGT-3' (Reverse). LMNB1 (9) and CTCF (10) were detected as previously described. CDKN2A, IL6, CXCL8, IL1A, IL1B, CXCL10, IFNA1 and IFNB1 were detected as previously described (2). The quantity of all samples was obtained using the standard curve method according to the manufacturer's protocol and was normalized to the housekeeping gene *ACTB.*

Northern Blot

Total RNA was extracted from proliferating or senescent TIG-3 and IMR-90/ER:H-Ras^{V12} cells by TRIzol Reagent (Invitrogen) according to manufacturer's protocols. After genomic DNA digestion using a TURBO DNA-*free* Kit (Applied Biosystems), total RNA samples (3–9 μg) were denatured in a 0.5 × MOPS (Nacalai Tesque), 2.2 M formaldehyde (Wako), and 50% formamide (Sigma-Aldrich) solution at 65°C for 15 minutes and then electrophoresed on 1% agarose gels containing 1× MOPS and 2.2 M formaldehyde solution (Wako). After transfer onto a Hybond-N+ membrane (Amersham/GE Healthcare) and followed by cross-linking with ultraviolet light, the membrane was prehybridized in Church buffer (11). A ^{32}P-labled DNA probe targeting hSATII RNA was generated from

the pcDNA3-hSATII RNA plasmid (described in the "Plasmid Construction" section) with the primer 5′-TATAATTCCA TTCGATTCC-3′ and the Megaprime DNA Labeling System (Amersham/GE Healthcare) according to manufacturer's protocols. The membrane was hybridized overnight with the purified probe using Sephadex G-50 DNA Grade NICK Columns (GE Healthcare) in Church buffer at 55°C. The membrane was then washed twice with 1× SSC buffer containing 0.1% SDS at 55°C for 5 minutes, followed by 0.2× SSC buffer containing 0.1% SDS at 55°C for 15 minutes. The hybridized ^{32}P signal was visualized on high-performance chemiluminescence film (Amersham/GE Healthcare).

RNA Pull-down Assay

RNA pull-down assays were performed using a RiboTrap Kit (MBL, #RN1011/RN1012) according to the manufacturer's instructions. Briefly, 5-bromo-UTP was randomly incorporated into hSATα, hSATII, MinSAT, and MajSAT RNAs upon transcription using vectors containing the full-length RNAs as templates (*in vitro* transcription). Next an anti-BrdU antibody conjugated with Dynabeads Protein G (Thermo Fisher Scientific, #10004D) were bound to the *in vitro*-synthesized RNA before incubating at 4°C for overnight with SVts8 cell lysates for hSATα and hSATII RNA or MEF lysates for MinSAT and MajSAT RNA. Finally, the samples were washed, eluted, and subjected to western blot or mass spectrometric analysis.

Western Blotting

Cell pellets were lysed in lysis buffer (0.1 M Tris-HCl pH 7.5, 10% glycerol, and 1% SDS), boiled for 5 minutes, and then centrifuged for 10 minutes at 15,000 rpm. All protein concentrations were determined by BCA Protein Assay Reagent (Pierce). Each cell lysate was electrophoresed by SDS-PAGE and transferred onto PVDF membranes (Millipore). After blocking with 5% skim milk (Megumilk) or 5% bovine serum albumin (Sigma-Aldrich) in Tris-buffered saline with 0.1% Tween 20 (TBST), the membrane was treated with primary antibodies to p16 (IBL, #11104, 1:250 dilution), lamin-B1 (Abcam, #ab16048, 1:1,000 dilution), GAPDH (Proteintech, #60004-1-lg, 1:10,000 dilution), vinculin (Sigma-Aldrich, #V9131, 1:1,000), CTCF (Cell Signaling Technology, #3418, 1:1,000 dilution), DDDK-tag (MBL, #M185-3L, 1:5,000), and ras (Oncogene, #OP41, 1:1,000 dilution) overnight at 4°C in blocking buffer. Membranes were then washed three times in TBST and incubated with an enhanced chemiluminescence (ECL) anti-mouse IgG, horseradish peroxidase-linked whole antibody (GE Healthcare, NA931V) or ECL anti-rabbit IgG, horseradish peroxidase-linked whole antibody (GE Healthcare, NA934V) for 1 hour at room temperature. After washing the membrane three times in TBST, the signal was resolved with SuperSignal West Femto Maximum Sensitivity Substrate (Thermo Fisher Scientific) and imaged on a FUSION imaging system (Vilber-Lourmat).

Mass Spectrometric Analysis

The hSATII RNA-binding proteins were purified using a RiboTrap Kit (MBL) as described in the "RNA Pull-down Assay" section. The eluate was then concentrated approximately 10-fold by Amicon Ultra 0.5 mL Centrifugal Filters (30K, Merck Millipore). Samples were reduced in 1× Laemmli sample buffer with 10 mM TCEP at 100°C for 10 minutes, alkylated with 50 mM iodoacetamide at ambient temperature for 45 minutes, and subjected to SDS-PAGE. Electrophoresis was stopped at a migration distance of 2 mm from the top

edge of the separation gel. After Coomassie Brilliant Blue staining, protein bands were excised, destained, and finely cut prior to in-gel digestion with Trypsin/Lys-C Mix (Promega) at 37°C for 12 hours. The resulting peptides were extracted from gel fragments and analyzed with an Orbitrap Fusion Lumos Mass Spectrometer (Thermo Scientific) combined with an UltiMate 3000 RSLC nano-flow HPLC (Thermo Scientific). Tandem mass spectrometry spectra were searched against a *Homo sapiens* protein sequence database in SwissProt using Proteome Discoverer 2.2 (Thermo Scientific), in which peptide identification filters were set at "false discovery rate (FDR) < 1%." Gene ontology analysis was performed by Metascape (12).

Chromatin Immunoprecipitation (ChIP) Followed by ChIP-Sequencing (ChIP-seq)

ChIP was essentially performed as described (2) with minor modifications. Briefly, cells at 70%–80% confluency were cross-linked with 1% formaldehyde for 10 minutes at room temperature and quenched with 125 mM glycine for 5 minutes at room temperature. The cross-linked cells were scraped into a microcentrifuge tube and washed twice with ice-cold phosphate-buffered saline (PBS). The washed cells were lysed in ChIP lysis buffer (1% SDS, 50 mM Tris-HCl pH 8.0, 10 mM EDTA, and 1× protease inhibitor cocktail) and then sonicated using a Bioruptor (Cosmo Bio Corporation) set to pulse on high (30 seconds of sonication, followed by 30 seconds of rest) at 4°C for 15 minutes. Lysates were cleared by centrifugation at maximum speed for 10 minutes at 4°C, and the chromatin-containing supernatants were transferred into to new centrifuge tube. After sixfold dilution with ice-cold ChIP dilution buffer (0.01% SDS, 1.1% Triton X-100, 1.2 mM EDTA, 16.7 mM Tris-HCl pH 8.0, 150 mM NaCl, and 1× protease inhibitor cocktail), the CTCF (Cell Signaling Technology, #3418) or Rabbit (DA1E) mAb IgG XP Isotype Control (Cell Signaling Technology, #3900) antibody was added, followed by overnight rotation at 4°C. The next day, samples were incubated with Dynabeads Protein G (Thermo Fisher Scientific, #10004D) at 4°C for 30 minutes before a wash process, according to the manufacturer's instruction. Dynabeads Protein G were collected on a magnet and washed three times with wash buffer I (0.1% SDS, 1% Triton X-100, 2 mM EDTA, 20 mM Tris-HCl pH 8.0, and 150 mM NaCl), wash buffer II (0.1% SDS, 1% Triton X-100, 2 mM EDTA, 20 mM Tris-HCl pH 8.0, and 500 mM NaCl), and wash buffer III (0.25% LiCl, 1% NP-40, 1% Na-DOC, 1 mM EDTA, and 10 mM Tris-HCl pH 8.0), followed by two washes with ice-cold TE (10 mM Tris-HCl pH 8.0 and 1 mM EDTA) and elution by ChIP elution buffer (1% SDS and 0.1 M Na_2CO_3). The eluted DNA was incubated overnight at 65°C for to reverse cross-links, followed by incubation in the presence of Proteinase K Solution (Wako) at 50°C for 2 hours. The samples were subsequently cleaned by phenol–chloroform extraction, precipitated with ethanol, and resuspended in either TE buffer for ChIP-qPCR or low TE buffer (10 mM Tris-HCl pH 8.0, and 0.1 mM EDTA) for ChIP-seq. ChIP-qPCR analyses were performed on a StepOne Plus PCR system (Thermo Fisher Scientific) using SYBR *Premix Ex Taq* II (Tli RNaseH Plus, TaKaRa, #RR820A). The primers used for qPCR are as follows: human imprinting control region (ICR): 5′-CCCATCTTGC TGACCTCAC-3′ (Forward) and 5′-AGACCTGGGA CGTTTCTGTG-3′ (Reverse) (13); hSATα: 5′-AAGGTCAATG GCAGAAAAGA A-3′ (Forward) and 5′-CAACGAAGGC CACAAGATGT C-3′ (Reverse); mouse ICR: 5′-GTCACTCAGG CATAGCATTC-3′ (Forward) and 5′-GTCTGCCGAG CAATATGTAG-3′ (Reverse) (14); MinSAT: 5′-

TTGGAAACGG GATTTGTAGA-3′ (Forward) and 5′-CGGTTTCCAA CATATGTGTT TT-3′ (Reverse).

Libraries for ChIP-seq were prepared with SMARTer ThruPLEX DNA-Seq Kit (Takara Bio USA) according to the manufacturer's protocol. The amplicon libraries for sequencing were quantified using a LabChip GX Touch (PerkinElmer) and sequenced using 2× 75-bp MiSeq Reagent Kits v3 (Illumina) on an Illumina MiSeq, according to the manufacturer's recommendations.

Chromosome Conformation Capture (3C)-qPCR

3C-qPCR was performed as previously described (15). In brief, to make a single-cell suspension hSATII RNA-overexpressed SVts8 cells were filtered through a 40-μm cell strainer and cross-linked with 1% formaldehyde for 10 minutes. After quenching with 125 mM glycine, the cross-linked cells were resuspended in lysis buffer (10 mM Tris-HCl pH 8.0, 10 mM NaCl, 0.2% NP-40, and 1× protease inhibitor cocktail) and subjected to enzymatic digestion using *Bgl*II (700 units, New England Biolabs) at 37℃ for overnight, followed by ligation with T4 DNA ligase (400 units, New England Biolabs) at 16℃ for 4 hours in a large volume. Next, cross-link reversal was performed by incubating samples overnight at 65°C in the presence of Proteinase K Solution (480 μg, Wako). The digested and ligated chromatin samples were then cleaned by phenol–chloroform extraction and precipitated with ethanol. The precipitated samples were subsequently cleaned using a QIAquick PCR Purification Kit (Qiagen) and resuspended in nuclease-free water. 3C-qPCR was performed using a StepOne Plus PCR system (Thermo Fisher Scientific) and SYBR *Premix Ex Taq* II (Tli RNaseH Plus, TaKaRa, #RR820A), and data were normalized to a GADPH control. The primers used for 3C-qPCR are as follows: 3C-Constant: 5'-CGGATAAGAG AAAGGAGGTG TTGG-3'; 3C-T1: 5'-AGGTGATGAA TCCTACCAGC AGTG-3'; 3C-T2, 5'-TGAGATTACA GGCATGAGCC AC-3'; 3C-T4: 5'-ATGTAGGGAA GTGATGGGAG AG-3'; 3C-T6: 5'-TACTGTTTCA AAGGCAGGCA CC-3'; 3C-T7: 5'-ACAACTGTCT TTCCCACCTA CC-3'; 3C-T15: 5'-GGGAGGAGAT TGACTACAAA GGAC-3'; 3C-T22: 5'-AGGTTGCAGT GAGCTGAGAT TG-3'; 3C-T26: 5'-AGACCCACTC ACAGAGATAA CC-3' and gGapdh-Fwd: 5'-GGGAGGTAGA GGGGTGATGT-3'; gGapdh-Rev: 5'-ATGGCATGGA CTGTGGTCTG-3'. The relative cross-linking frequency was calculated by setting the cross-linking frequency of a bacterial artificial chromosome-containing amplified locus at 100%.

Assay for Transposase-Accessible Chromatin (ATAC)-seq

ATAC-seq was performed as previously described (16). The amplicon libraries for sequencing were quantified using a LabChip GX Touch (PerkinElmer) and KAPA Library Quantification Kit (KAPA Biosystems, #KK4824) and sequenced using 2 × 75-bp MiSeq Reagent Kits v3 (Illumina) on an Illumina MiSeq, according to the manufacturer's recommendations.

RNA Immunoprecipitation (RIP)

To evaluate the binding of CTCF and hSATII RNA, HEK-293T cells were transfected with vector constructs designed to express either CTCF (WT) or CTCFΔZF and hSATII RNA using X-tremeGENE HP DNA Transfection Reagent (Roche), according to the

manufacturer's instructions. After 24 hours, the cells were scraped and lysed, followed by RIP assay. XRA-induced senescent IMR-90 cells were infected by lentiviruses with 10 μg/mL polybrene on Day 8 after XRA irradiation. The infected cells were then scraped on Day 10 and lysed, followed by RIP assay. RIP assay was performed using a Magna RIP RNA-Binding Protein Immunoprecipitation Kit (Millipore, #17-700) according to the manufacturer's instructions. After removing genomic DNA contamination using a TURBO DNA-*free* Kit (Applied Biosystems), immunoprecipitated RNA underwent subjected to reverse transcription using a PrimeScript RT Master Mix (TaKaRa). Next, qPCR was performed to quantify the immunoprecipitated RNA using a StepOne Plus PCR system (Thermo Fisher Scientific) and SYBR *Premix Ex Taq* II (Tli RNaseH Plus, TaKaRa, #RR820A). The primers used for qPCR are listed in the "RT-qPCR" and "Chromatin Immunoprecipitation (ChIP) Followed by ChIP Sequencing (ChIP-seq)" sections. The percent input (% Input) was calculated.

Electrophoretic Mobility Shift Assay (EMSA)

Human full-length CTCF cDNA was cloned into a pGEM-6P-1 plasmid (GE Healthcare) to produce recombinant CTCF with glutathione S-transferase (GST)-tagged N-terminal (GST-CTCF). The plasmid was transformed into *Escherichia coli* BL21 host strains (TaKaRa), and GST-CTCF expression was induced under 0.2 M isopropyl β-D-thiogalactopyranoside and 100 μM $ZnSO_4$ at 20°C for 2 hours. After collecting *E. coli* cells by centrifugation, the pellet was resuspended in PBS containing 1× protease inhibitor cocktail, followed by sonication using a Bioruptor (Cosmo Bio Corporation) set to pulse on high (20 seconds of sonication, followed by 30 seconds of rest) at 4°C for 3 minutes. GST-CTCF was purified by GST Sepharose 4B (GE Healthcare), followed by GST-tag removal using a PreScission Protease (GE Healthcare) according to the manufacturer's protocol. hSATII and hSATα RNAs were transcribed *in vitro* by a MEGAscript Kit (Invitrogen/ Thermo Fisher Scientific). EMSA was performed using a LightShift Chemiluminescent EMSA Kit (Thermo Fisher Scientific) according to the manufacturer's protocol. Briefly, recombinant CTCF was purified as described, and 10 fmol/μL biotin-labeled ICR probe (17) and/or hSATII or hSATα RNA at a concentration of 10, 5, or 2.5 pmol/μL were incubated for 20 minutes at room temperature. After incubation, the mixture was loaded on a 5% polyacrylamide gel and underwent electrophoresis (100 V) at 4°C for 110 minutes in 0.5× TBE. After transfer onto a Hybond-N+ membrane (Amersham/GE Healthcare), samples were cross-linked with ultraviolet light. The signals of biotin-labeled probes were detected using a Chemiluminescent Nucleic Acid Detection Module Kit (Thermo Fisher Scientific) according to the manufacturer's protocol. Chemiluminescence signals were detected using a FUSION imaging system (Vilber-Lourmat).

Immunofluorescence Imaging

To detect multipolar or chromosomal bridge formation, hSATII RNA-expressing SVts8 or MajSAT RNA-expressing MEFs were seeded on PLL-coated glass cover slips (Matsunami Glass, #C1210). After 24 hours, the cells were fixed with ice-cold methanol at -20°C for 10 minutes, and permeabilized with 0.1% Triton X-100. After blocking with 15% goat serum (Sigma-Aldrich, #G9023), cells were incubated with α-tubulin (Sigma-Aldrich, #T9026, 1:5,000), γ-tubulin (Sigma-Aldrich, #T3559, 1:5,000), or pericentrin (Abcam, #ab4448, 1:1,000) antibodies overnight at 4°C. The next day, the blots were washed twice

with PBS and then incubated with a Goat anti-Rabbit IgG (H+L) Cross-Adsorbed Secondary Antibody, Alexa Fluor 488 (Thermo Fisher Scientific, #A11008, 1:1,000) and Goat anti-Mouse IgG (H+L) Highly Cross-Adsorbed Secondary Antibody, Alexa Fluor 594 (Thermo Fisher Scientific, #A11032, 1:1,000) at room temperature for an hour. The slides were mounted using ProLong Diamond Antifade Mountant with DAPI (Thermo Fisher Scientific) and examined using a BZ-X710 fluorescence microscope (Keyence).

Karyotype Analysis

Cells were treated with nocodazole (100 ng/mL) for 12 (MEFs) or 4 (SVts8) hours. Karyotype analysis of mitotic cells was performed as previously described (18).

Focus Formation Assay

MajSAT RNA-expressing MEFs ($1–5\times 10^4$) previously described in the "RNA Interference (RNAi) and Overexpression" section were seeded into 6-cm-diameter dishes. The cells were maintained at physiological oxygen conditions (92% N_2, 5% CO_2, and 3% O_2) for approximately a month, and the medium was changed weekly until the cells were photographed and counted. After the approximately 1-month culture, cells were stained with 0.05% crystal violet in 20% methanol. Dishes were scanned, and piled-up foci were counted.

Anchorage-Independent Soft Agar Colony Formation Assay

A total of 1×10^3 cells were suspended in DME medium containing 0.4% SeaPlaque Agarose (Lonza, #50101) and 10% FBS and layered on DME medium containing 0.6% SeaPlaque Agarose and 10% FBS in 6-well plates in triplicate. After 2–3 weeks of incubation, the number of colonies was counted.

RNA Sequencing (RNA-Seq)

Total RNA was extracted from satellite RNA-overexpressed or XRA-irradiated (12 Gy) SVts8 cells using TRIzol Reagent (Invitrogen), details of which are found in the "Cell Culture" or "RNA Interference (RNAi) and Overexpression" sections. After genomic DNA digestion using a TURBO DNA-*free* Kit (Applied Biosystems), sequencing libraries were prepared using a NEBNext Ultra RNA Library Prep Kit for llumina (New England Biolabs) according to the manufacturer's instruction, followed by 150-bp paired-end sequencing performed by Annoroad Corporation using a HiSeq X.

Extraction and Application of Exosome-Like Extracellular Vesicles (EVs)

To cause DXR-induced senescence, RPE-1/hTERT cells were cultured in medium containing DXR at concentrations of 150 ng/mL. One day before DXR treatment, RPE-1/hTERT cells were plated at a density of 3,637 cells•cm^{-2}. These cells were not passaged after DXR treatment. To induce XRA-induced senescence, RPE-1/hTERT cells were exposed to 40-Gy irradiation with a CP-160 X-ray machine (Faxitron X-ray Corporation). After XRA irradiation, RPE-1/hTERT cells were plated at a density of 4,000 cells•cm^{-2}. These cells were not passaged for 10 days after XRA irradiation. EVs were collected from senescent RPE-1/hTERT cells cultured for 3 days in DME medium containing 5% FBS by EV depletion using ultracentrifugation at 100,000 × g for 16 hours. The number of EVs was counted using a LM10 Nanoparticle Characterization System (NanoSight) as

previously described (3, 4). The total RNA of EVs was extracted using TRIzol LS Reagent (Thermo Fisher Scientific) according to the manufacturer's protocols. Regarding the addition of EVs to cells, after the collected EVs were mixed in FBS-depleted medium at a density of 2×10^9 particles/mL, the medium of host cells was changed with the EV-containing medium daily for one week. Subsequently, karyotyping or anchorage-independent growth assay of EV-treated cells were performed. Designer exosome production using EXOtic devices was performed as previously reported (19), and EV extraction and application to cells were similarly performed as described.

RNA *In Situ* Hybridization (RNA-ISH)

Tissue samples were obtained from a patient who underwent surgical resection at Cancer Institute, Japanese Foundation for Cancer Research (JFCR). Tissue samples were collected after obtaining the appropriate institutional review board approval (approval number: 2013–1090) and written informed consent of the patient. hSATII RNA was detected on formalin-fixed paraffin-embedded (FFPE) sections in primary colon cancer specimens using an Advanced Cell Diagnostics (ACD) RNAscope® 2.5 HD Reagent Kit-BROWN (ACD, #322300) and the RNAscope® Target Probe - Hs-HSATII (ACD, #504071) according to the manufacturer's instructions. For each sample (n = 10), two images (×100) of normal mucosa, submucosa and tumor were randomly selected. The area of hSATII RNA positivity and total cells were analyzed using NIH ImageJ software. The hSATII RNA-positive area per field (%) of each type of cell was calculated as the proportion of the total positive area to the total area of cells.

Organoid Culture Experiments

Organoids prepared from small intestinal tumors ($Apc^{\Delta 716}$ or $Apc^{\Delta 716}$ $Trp53^{R270H/R270H}$) were cultured as previously described (20). Total RNA was collected using an RNeasy Plus Micro Extraction Kit (Qiagen) after organoid culture for 3 days.

***In Vivo* Allograft Assays**

MEF/Vector or MEF/MajSAT RNA (5×10^6 cell) in Hank's Balanced Salt Solution (Gibco/Thermo Fisher Scientific) were subcutaneously injected with an equal volume of Matrigel (BD Pharmingen) into 4- or 5-week-old female BALB/c-nu/nu mice (Charles River Laboratories). After 20 or 30 days of cell injection, the mice were euthanized, and tumor weight was measured. All animal procedures were performed using protocols approved by the JFCR Animal Care and Use Committee in accordance with the relevant guidelines and regulations (approval number: 1804-05).

Bioinformatical Analysis

The sequence and processing data have been deposited in the DNA Data Bank of Japan with the accession numbers DRA009771 (https://ddbj.nig.ac.jp/DRASearch/submission?acc=DRA009771) for RNA-seq, DRA010750 (https://ddbj.nig.ac.jp/DRASearch/submission?acc=DRA010750) for ChIP-seq, and DRA010749 (https://ddbj.nig.ac.jp/DRASearch/submission?acc=DRA010749) for ATAC-seq. All other data supporting the findings of this study are available within the article.

Screening for unique transcripts showing increased chromatin accessibility and active transcription

To screen for loci showing increased chromatin accessibility and being actively transcribed during cellular senescence (**Fig. 1*A***), we first performed a comparative analysis of ATAC-seq data between proliferating and X-ray-induced senescent IMR-90 cells. The resulting paired-end FastQ reads of ATAC-seq underwent quality control with FastQC (version 0.11.8) and trimmed with TrimGalore (version 0.6.4; https://www.bioinformatics.babraham.ac.uk/projects/trim_galore/). The trimmed reads were mapped against *Homo sapiens* UCSC hg19 using Bowtie 2 (version 2.3.5) alignment software (21). SAMtools (version 1.9) was used to sort and convert SAM to BAM files (22, 23). Uniquely mapped reads were used for peak calling using MACS 2 (version 2.1.4) with the command "$ macs2 callpeak --nomodel --nolambda --keep-dup all --call-summits -f BAMPE -g hs," and peaks were filtered by an enrichment score ($q < 0.01$) (24). Using the read-depth normalized matrix of ATAC-seq signal for all consensus peaks, differential loci of chromatin accessibility between proliferating and X-ray-induced senescent IMR-90 cells were determined using DiffBind (version 2.14.0), resulting in 16,325 peaks displaying significantly altered chromatin accessibility, FDR < 0.05 and region width < 10 k based on the consensus peaks identified in at least two replicates. Based on 14,356 and 1969 of the 16,325 peaks showing "Up"- and "Down"-regulated in X-ray-induced senescent IMR-90 cells compared to proliferating IMR-90 cells, respectively. We defined the total 16,325 peaks as "Differential Peaks" (**Fig. 1*A* and *B***). Peak distributions showing significantly altered chromatin accessibility in the senescent cells (*SI Appendix,* Fig. S1*A*) were analyzed by the *cis*-regulatory element annotation system (25).

Next, to identify transcripts containing the 16,325 regions displaying significantly altered chromatin accessibility in X-ray-induced senescent IMR-90 cells, we referred to GRCh37/hg19 and RepeatMasker databases using BEDTools (26), resulting in the identification of 652 transcripts in these regions. The referral GRCh37/hg19 database was from the UCSC genome annotation database for the February 2009 assembly of the human genome (hg19, GRCh37 Genome Reference Consortium Human Reference 37), whereas the RepeatMasker database [DNA, LINE, LTR, RC, RNA (7SK), rRNA, Satellite, SINE and snRNA families] was referred from hg19 - February 2009 - RepeatMasker open-4.0.5 - Repeat Library 20140131.

We then calculated the gene expression level of these 652 transcripts in proliferating and X-ray-induced senescent IMR-90 cells. Publicly available data of proliferating and senescent IMR-90 cells (GEO: GSE130727) (27) were reanalyzed using four samples: GSM3752532 (IMR-90 PDL15 1) and GSM3752533 (IMR-90 PDL15 2) for proliferating IMR-90 cells and GSM3752534 (IMR-90 IR+ 1) and GSM3752535 (IMR-90 IR+ 2) for X-ray-induced senescent IMR-90 cells. For comparative analysis of RNA-seq, we used original datasets from published data as internal controls. In the transcriptome analysis of coding genes and some noncoding RNAs, the trimmed paired-end FastQ reads by TrimGalore (version 0.6.4) were aligned to a comprehensive gene annotation file (GENCODE, GRCh37, release 34) using HISAT2 (version 2.1.0) (28) using default settings. SAMtools (version 1.9) was used to sort and convert SAM to BAM files (22, 23). The counts mapped to the transcripts were computed using featureCounts (29). In the transcriptome analysis of repetitive elements, the trimmed paired-end FastQ reads by TrimGalore (version 0.6.4) were mapped against *H. sapiens* UCSC hg19 using the Bowtie

2 (version 2.3.5) alignment software (21). The counts of repetitive elements were calculated by *RepEnrich2* (30) using default settings. These counts (coding genes, some noncoding RNAs and repetitive elements) were then normalized using the trimmed mean of M-values method in EdgeR (version 3.28.1) (31). Among the 652 transcripts, 47 differentially expressed transcripts were identified (significance determined with FDR < 10^{-10}) and are shown as red (upregulated; 32 transcripts) or blue (downregulated; 15 transcripts) dots in the volcano plot (**Fig. 1*C***).

The volcano plots were visualized using the "ggplot2" package (**Fig. 1*B*** and ***C***). The peaks of uniquely mapped reads by ATAC-seq and RNA-seq in hSATII loci are shown using the Integrative Genomics Viewer for visualization (**Fig. 1*D***) (32, 33).

RNA-seq analysis

For RNA-seq analysis in hSATα- or hSATII-overexpressed and X-ray-induced senescent SVts8 cells (**Fig. 1*E*–*G***; *SI Appendix*, Fig. S2*B*–*D*), the resulting FastQ reads containing more than 50% of below Q20 and more than 5% of N were removed, as performed by Annoroad Corporation. The trimmed reads were aligned to a comprehensive gene annotation file (GENCODE, GRCh37, release 34) using HISAT2 (version 2.1.0) (28) using default settings, and the number of transcripts per kilobase million (TPM) was estimated by StringTie (version 2.0) (34). To summarize and visualize RNA-seq data in hSATα- or hSATII-overexpressed and X-ray-induced senescent SVts8 cells, principal component analysis was performed using singular value decomposition approach implemented in R function (prcomp) on TPM values (*SI Appendix*, Fig. S2*C*). For comparative analysis of RNA-seq, we used original datasets from our RNA-seq data as internal controls. Each heatmap column regarding SASP-related gene expression in hSATα- or hSATII-overexpressed and X-ray-induced senescent SVts8 cells shows the value normalized to a *z*-score using each TPM value (Fig. **1*E***). Gene Set Enrichment Analysis (GSEA; **Fig. 1*G***; *SI Appendix*, Fig. S2*D*) was carried out using the GSEA tool from the Broad Institute (35). The scatter plots (**Fig. 1*F***; *SI Appendix*, Fig. S2*B*) were visualized using the "ggplot2" package.

For RNA-seq analysis in cells, multivesicular endosomes (MVEs) or exosomes derived from DKO1 (human colon cancer cell line; *SI Appendix*, Fig. S7*A*), publicly available data (GEO: GSE130727) (36) were reanalyzed using 12 samples; GSM3584509 (DKO1_Exo_Cell_RNA_1), GSM3584510 (DKO1_Exo_Cell_RNA_2), GSM3584511 (DKO1_Exo_Cell_RNA_3), and GSM3584512 (DKO1_Exo_Cell_RNA_4) for cells; GSM3584513 (DKO1_Exo_MV_RNA_1), GSM3584514 (DKO1_Exo_MV_RNA_2), GSM3584515 (DKO1_Exo_MV_RNA_3), and GSM3584516 (DKO1_Exo_MV_RNA_4) for MVEs; and GSM3584517 (DKO1_Exo_Low_RNA_1), GSM3584518 (DKO1_Exo_Low_RNA_2), GSM3584519 (DKO1_Exo_Low_RNA_3), and GSM3584520 (DKO1_Exo_Low_RNA_4) for exosomes. For comparative analysis of RNA-seq, we used original datasets from published data as internal controls. The trimmed paired-end FastQ reads by TrimGalore (version 0.6.4) were mapped against *H. sapiens* UCSC hg19 using the Bowtie 2 (version 2.3.5) alignment software (21). The counts of repetitive elements were calculated by *RepEnrich2* (30) using default settings. Counts per million are shown (*SI Appendix*, Fig. S7*A*).

ATAC-seq analysis

For ATAC-seq analysis in empty vector- or hSATII-overexpressed SVts8 cells (**Fig. 3*E***), the resulting FastQ reads underwent quality control with FastQC (version 0.11.8) and trimmed with TrimGalore (version 0.6.4). The trimmed sequences were mapped against *H. sapiens* UCSC hg19 using Bowtie 2 (version 2.3.5) alignment software (21). Uniquely mapped reads were used for peak calling using MACS 2 (version 2.1.4) with the command "$ macs2 callpeak --nomodel --nolambda --keep-dup all --call-summits -f BAMPE -g hs," and peaks were filtered by an enrichment score ($q < 0.01$) (24). Each specific peak was identified using BEDTools using intersect.

ChIP-seq analysis

For ChIP-seq analysis (Fig. **3*A*–*C***, **3*E***), FastQ reads underwent quality control with FastQC (version 0.11.8) and trimmed with TrimGalore (version 0.6.4) using default settings. The trimmed sequences were mapped against *H. sapiens* UCSC hg19 using Bowtie 2 (version 2.3.5) alignment software (21). Uniquely mapped reads were used for peak calling using MACS 2 (version 2.1.4), and the peaks were filtered by an enrichment score ($p < 0.001$) (24). The 36,084 specific peaks detected in empty vector-expressed SVts8 cells or the 33,941 specific peaks detected in hSATII RNA-overexpressed SVts8 cells were identified using BEDTools using intersect. Normalized bigwigs were generated by deepTools (version 3.5.1) (37) "computeMatrix" command and the tracks in chr4: 76,930,000 to 77,030,000 were visualized with RNA-seq and ATAC-seq data using Integrative Genomics Viewer (Fig. **3*E***) (32, 33). For the enrichment of peaks from ChIP-seq data, we used deepTools to generate read abundance from all datasets around peak center ± 2-kb region, using "computeMatrix." These matrices were then used to create profiles (Fig. **3*B***, left) and heatmaps (Fig. **3*B***, right) split into two clusters using the k-means algorithm using deepTools commands "plotProfile" or "plotHeatmap," respectively.

Statistical Analysis

Parametric statistical analyses were performed using the unpaired two-tailed Student's *t*-test (**Fig. 3*F***; *SI Appendix*, Fig. S1*C* and S3 *G*, *I*, *J*, and *L*, and S5 *B*–*E*, S6 *B*–*E*, and S7 *E*–*G*), or one-way analysis of variance (ANOVA), followed by the Dunnett's (**Fig. 2*F*** and **4*A***; *SI Appendix*, Fig. S2*A* and S7*C)* or Tukey's (**Fig. 1*H*** and **2*D*** and ***E*** and **3*C***; *SI Appendix*, Fig. S2 *E* and *F* and S3*C* and *D* and S5*G*) multiple comparisons post hoc test using the R software for statistical computing (64-bit version 3.6.1). Non-parametric statistical analyses were performed using the Wilcoxon rank-sum test (**Fig. 3*B*** and **4*D*–*E***), or the Kruskal-Wallis *H* test (one-way ANOVA on ranks) followed by the Steel's multiple comparisons post hoc test (*SI Appendix*, Fig. S6*F*) using the R software for statistical computing. A *P*-value < 0.05 was considered statistically significant. All experiments, except for mass spectrometric analysis, were repeated at least twice.

Statistical Analysis

Parametric statistical analyses were performed using the unpaired two-tailed Student's *t* test (Fig. 3*F* and *SI Appendix*, Figs. S1*C*, S3 *G*, *I*, *J*, and *L*, S5 *B*–*E*, S6 *B*–*E*, and S7 *E*–*G*) or one-way ANOVA, followed by the Dunnett's (Figs. 2*F* and 4*A* and *SI Appendix*, Figs. S2*A* and S7*C*) or Tukey's (Figs. 1*H*, 2 *D* and *E*, and 3*C* and *SI Appendix*, Figs. S2 *E* and *F*, S3 *C* and *D*, and S5*G*) multiple comparisons post hoc test using the R software for statistical computing (64-bit version 3.6.1). Nonparametric statistical analyses were

performed using the Wilcoxon rank-sum test (Figs. 3*B* and 4 *D* and *E*) or the Kruskal–Wallis *H* test (one-way ANOVA on ranks) followed by the Steel's multiple comparisons post hoc test (SI Appendix, Fig. S6*F*) using the R software for statistical computing. $P < 0.05$ was considered statistically significant. All experiments, except for mass spectrometric analysis, were repeated at least twice.

Figure. S1

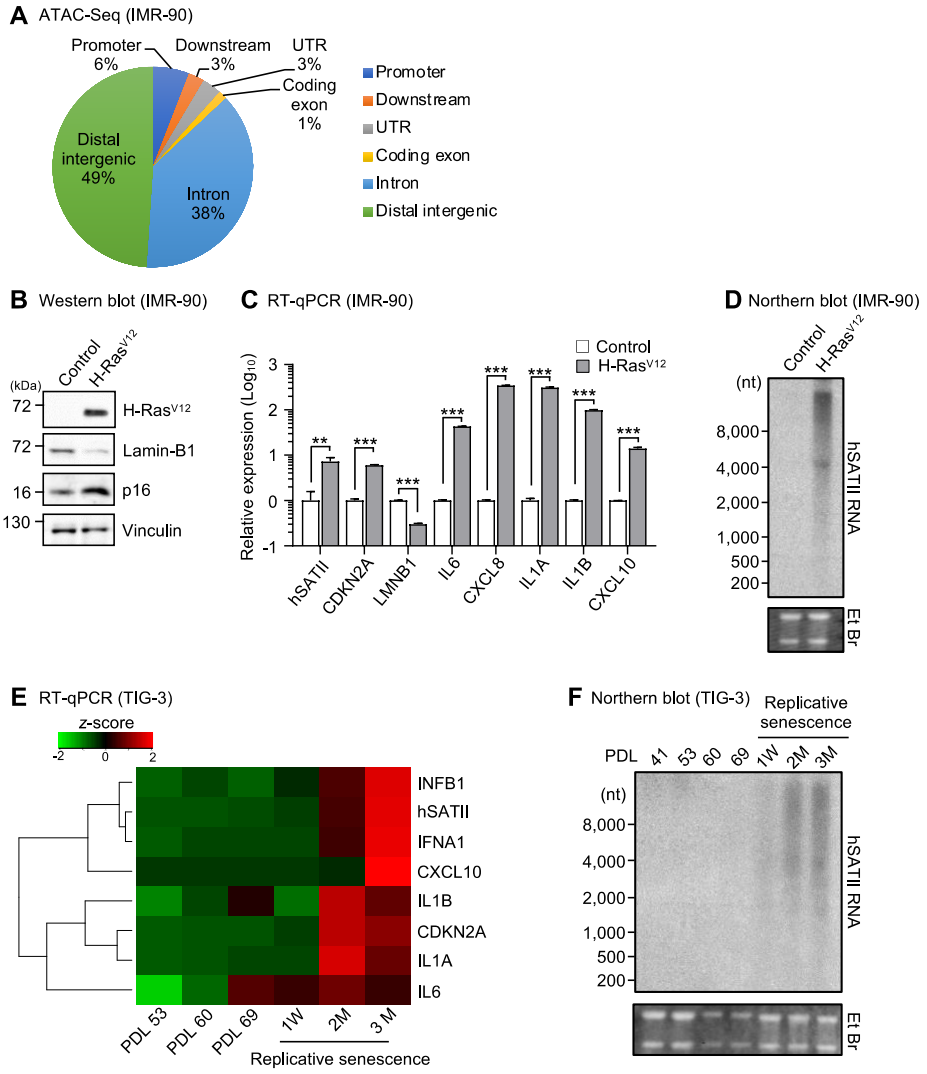

Fig. S1. Pericentromeric satellite RNA is upregulated during cellular senescence.

(**A**) Peak distribution of the 16,325 regions dramatically altered (FDR < 0.05) during cellular senescence in IMR-90 cells by ATAC-seq (**Fig. 1*A*** and ***B***). (**B–F**) Pre-senescent cells were rendered senescent by treatment with 4-OHT to activate oncogenic H-Ras^{V12} (IMR-90/ER:H-Ras^{V12}, **B–D**) or serial passage (TIG-3, **E** and **F**). These cells were subjected to Western blotting (**B**), RT-qPCR (**C** and **E**), and Northern blot (**D** and **F**) to detect hSATII RNA and senescence markers. Replicative senescent cells rendered senescent by serial passage were collected at 1 week (W), 2 months (M), and 3 months after the cessation of proliferation (**E** and **F**). PDL, population doubling level. The relative expression indicates the value normalized to that of proliferating (control) cells (**C**). Each bar represents mean ± SD of three technical replicates repeated in two independent experiments (**C**). Each column shows the values normalized to *z*-score after calculated as a fold change from proliferating (PDL 41) TIG-3 cells (**E**). ***P < 0.001 by the unpaired two-sided *t*-test.

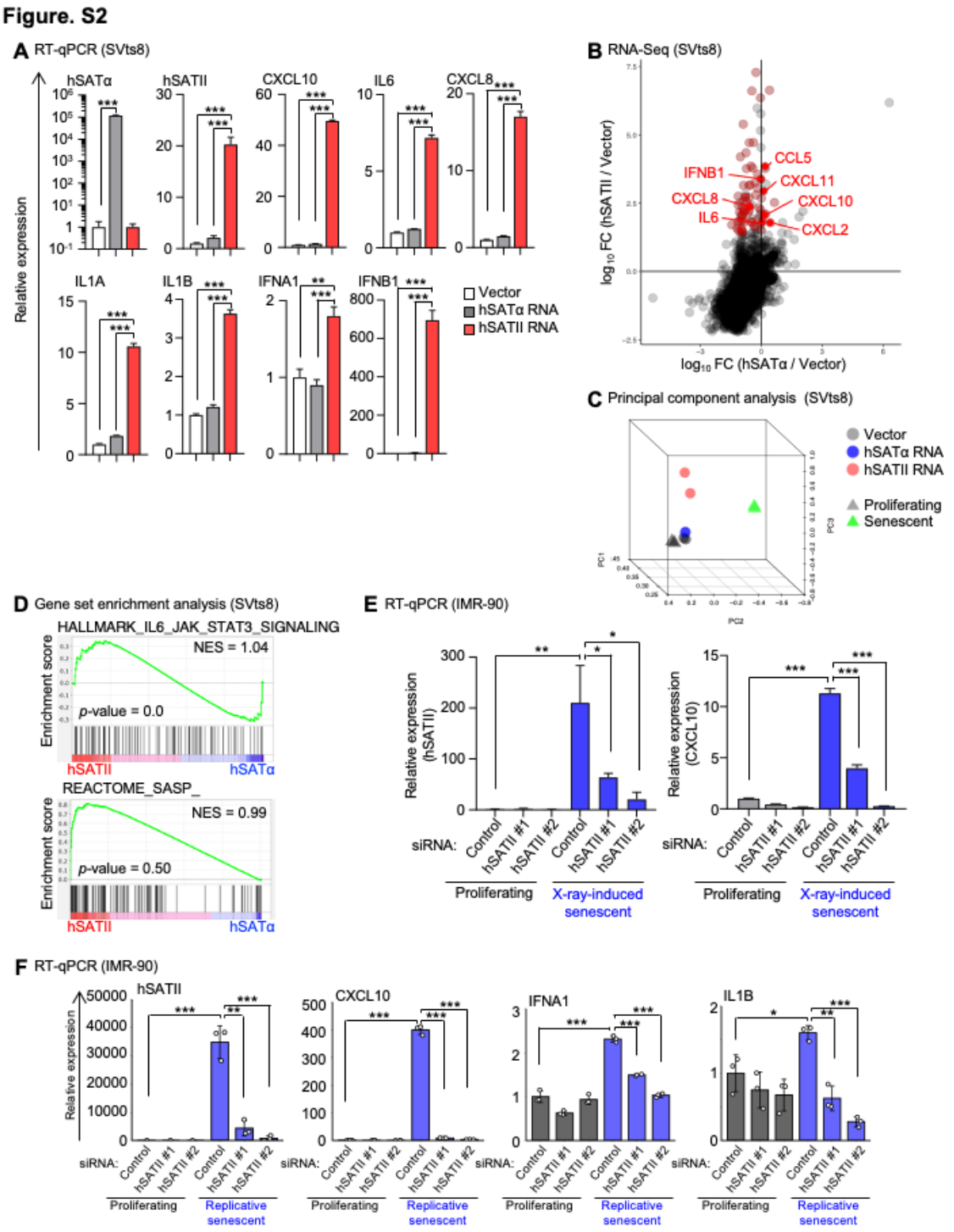

Fig. S2. Pericentromeric satellite RNA promotes SASP-like inflammatory gene expression.

(**A**) RT-qPCR analysis of SASP-like inflammatory genes in hSATα- and hSATII RNA-overexpressing SVts8 cells. The relative expression indicates the value normalized to that of empty vector-expressed cells. (**B**) Scatterplot showing the biological replicate in **Fig. 1*F***. (**C**) PCA of RNA-seq performed in **Fig. 1*E***. (**D**) GSEA of signatures associated with

IL6-JAK-STAT3 and SASP in hSATII RNA-overexpressed SVts8 cells. NES, normalized enrichment score. (**E** and **F**) The effect of the knockdown of hSATII RNA on the expression level of hSATII RNA and SASP-like inflammatory genes in proliferating (control) and X-ray-induced (**E**) or replicative senescent (**F**) IMR-90 cells. The relative expression shows a value normalized to that of control siRNA-treated proliferating cells. Each bar represents mean ± SD of three technical replicates, repeated in two independent experiments (**A**, **E**, **F**). $*P < 0.05$, $**P < 0.01$ or $***P < 0.001$ by one-way ANOVA followed by the Dunnett's multiple comparisons post hoc test (**A**) or Tukey's multiple comparisons post hoc test (**E**, **F**).

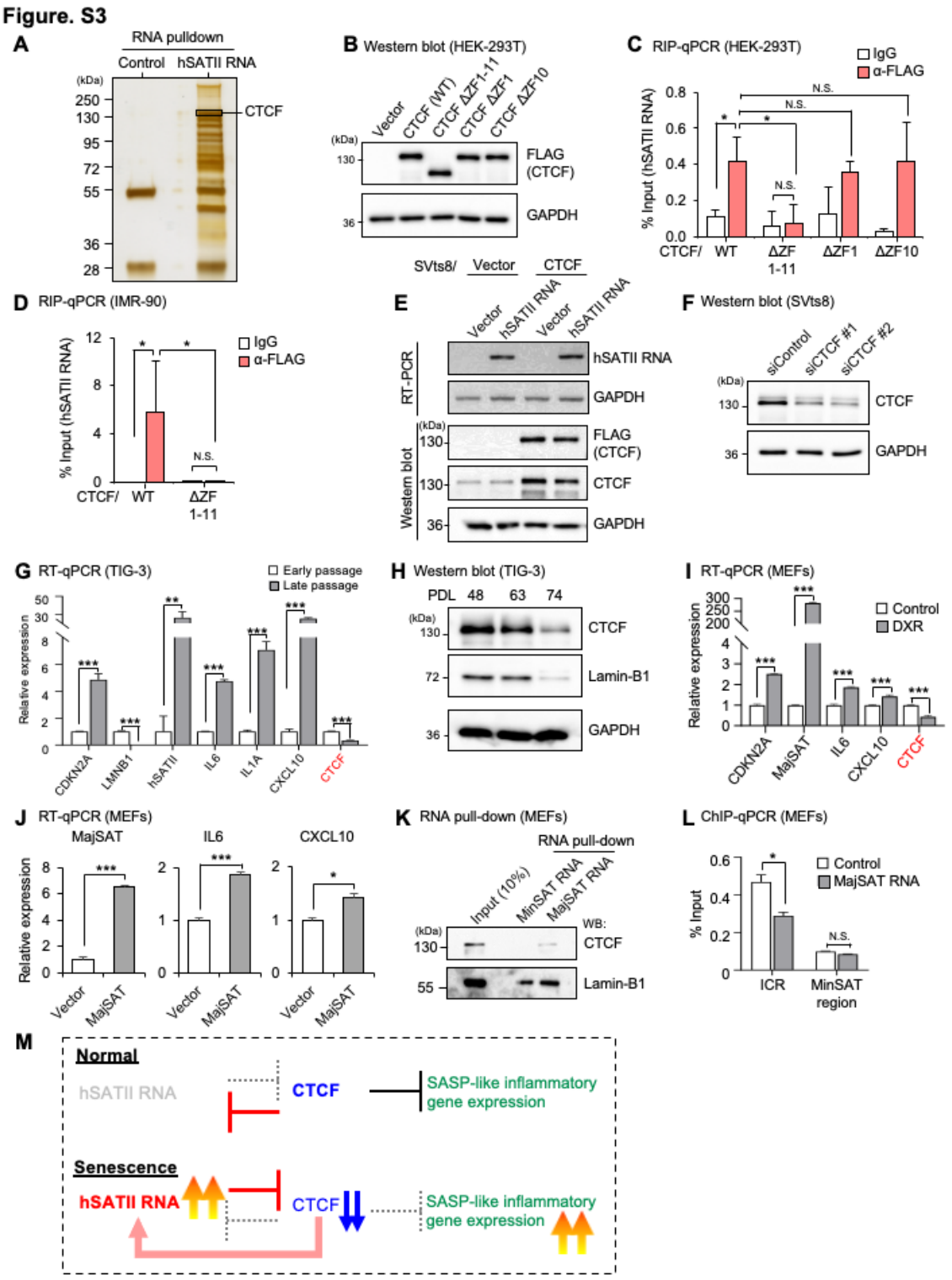

Fig. S3. Pericentromeric satellite RNA is bound to CTCF and regulated by CTCF.

(**A**) Silver staining for hSATII RNA-binding proteins. (**B** and **C**) Western blot analysis of FLAG-tagged CTCF (WT: wild type), CTCFΔZF1-11 (deletion of ZF domains 1-11), CTCFΔZF1, or CTCFΔZF10 (**B**) and RIP assay (**C**) of HEK-293T cells. (**D**) RIP assay of

X-ray-induced senescent IMR-90 cells overexpressing FLAG-tagged CTCF or CTCFΔZF1-11. (**E**) RT-PCR analysis of hSATII RNA, and Western blot analysis using antibodies; anti-FLAG (CTCF), anti-CTCF and anti-GAPDH. (**F**) Western blot analysis of CTCF knockdown by siRNA. (**G** and **H**) RT-qPCR (**G**) or Western blot (**H**) analysis of hSATII RNA, CTCF, and SASP genes in serial passage-induced senescent TIG-3 cells. The relative expression shows the value normalized to that of early-passage cells. (**I** and **J**) RT-qPCR analysis of MajSAT RNA and SASP-like inflammatory genes in DXR-induced senescent MEFs (**I**) or MajSAT RNA-expressing MEFs (**J**). The relative expression indicates the value normalized to that of control treatment (**I**) or empty vector-expressed (**J**) cells. (**K**) Immunoprecipitated proteins bound to MinSAT or MajSAT RNA. (**L**) ChIP-qPCR analysis for CTCF binding to ICR or MinSAT locus. (**M**) Scheme of hSATII RNA regulation by CTCF. Although CTCF normally suppresses the expression of hSATII RNA and SASP-like inflammatory genes at a low level, the reduction of CTCF provokes the expression of hSATII RNA during cellular senescence. Subsequently, the upregulated hSATII RNA disturbs CTCF binding to DNA, which induces SASP-like inflammatory gene expression. Each bar represents mean ± SD of three technical replicates repeated in two independent experiments (**C**, **D**, **G**, **I**, **J**, **L**). $*P < 0.05$, $**P < 0.01$, $***P < 0.001$ or N.S. (not significant) by the one-way ANOVA followed by the Tukey's multiple comparisons post hoc test (**C**, **D**) or the unpaired two-sided *t*-test (**G**, **I**, **J**, **L**).

Figure. S4

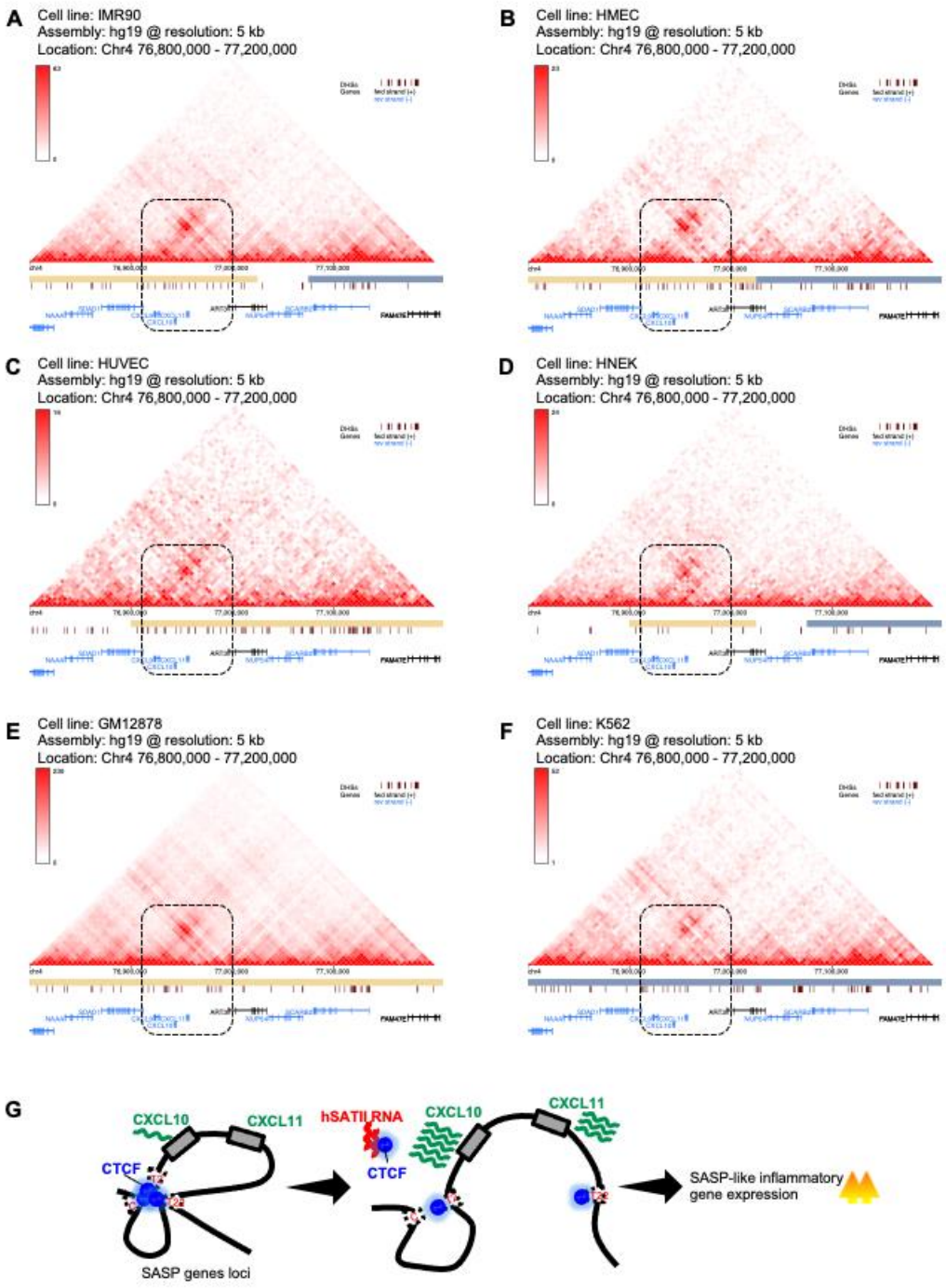

Fig. S4. Pericentromeric satellite RNA provokes a change of chromatin interaction at *CXCL10/11* loci.

(**A**–**F**) Hi-C data in IMR90 (**A**), HMEC (**B**), HUVEC (**C**), HNEK (**D**), GM12878 (**E**), and K562 (**F**) cells (assembly: hg19, location: chr4 76,800,000-77,200,000) were obtained from 3D Genome browser (38, 39). The region considered in 3C assay (**Fig. 3*F***) is surrounded by a broken line. (**G**) A predictive model of hSATII RNA-induced SASP-like

inflammatory gene expression by the disruption of CTCF-sustained chromatin organization.

Figure. S5

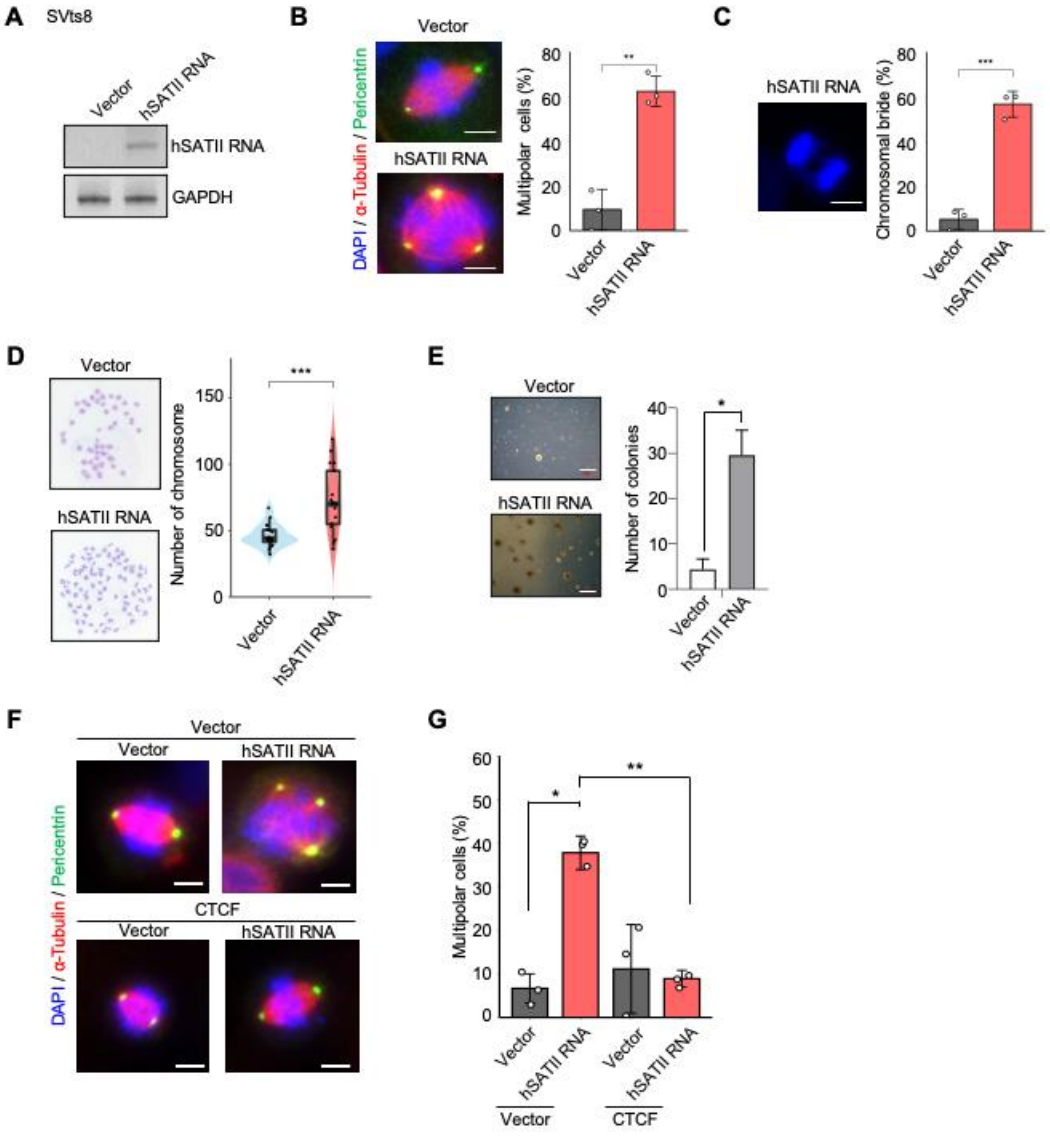

Fig. S5. Pericentromeric human satellite RNA provokes chromosomal instability.

(**A**) The retrovirus transduction of hSATII RNA in SVts8 cells was validated by RT-PCR. (**B** and **C**) Immunostaining of SVts8 cells for microtubules (α-tubulin), centrosomes (pericentrin), and DNA (DAPI). Percentage of multipolar cells (**B**) or chromosome-bridged cells (**C**). Scale bar, 5 μm. Each bar represents mean ± SEM of three biological replicates (total of 90 cells per condition). (**D** and **E**) Karyotype analysis (n = 20) (**D**) and anchorage-independent growth analysis (**E**) of hSATII RNA-overexpressed SVts8 cells. Scale bar, 500 μm. Data are mean ± SEM (n = 3, total of 15 independent fields per condition). (**F** and **G**) Immunostaining (**F**) and percentage of multipolar cells (**G**) in SVts8 cells. Scale bar, 5 μm. Each bar represents mean ± SEM of three biological replicates (total of 90 cells per condition). **P* < 0.05, ***P* < 0.01, or ****P* < 0.001 by the unpaired two-sided *t*-test (**B**, **C**, **D**, **E**) or one-way ANOVA followed by the Tukey's multiple comparisons post hoc test (**G**).

Figure. S6

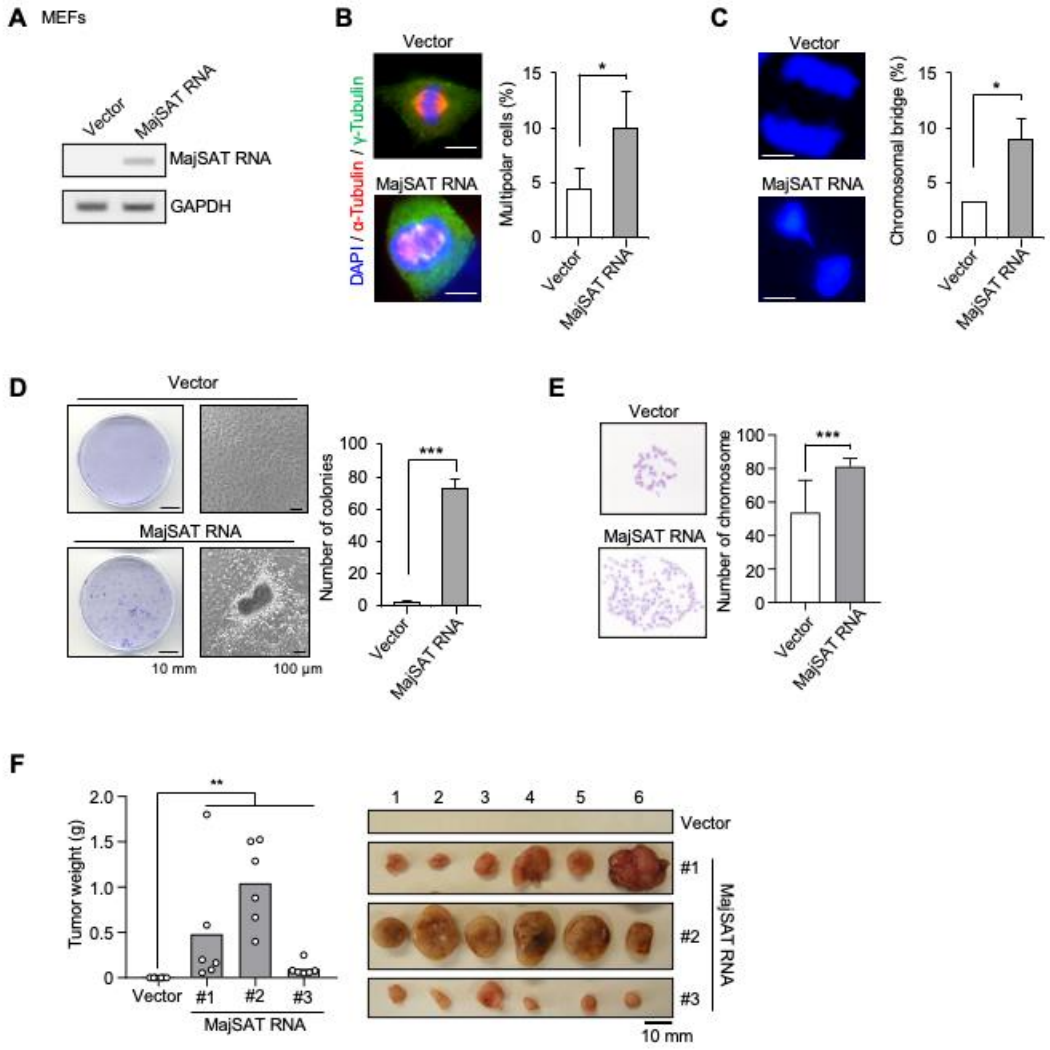

Fig. S6. Pericentromeric mouse satellite RNA provokes chromosomal instability.

(**A–C**) RT-PCR of MajSAT RNA overexpression in MEFs (**A**). Immunostaining for microtubules, centrosomes and DNA. Percentage of multipolar cells (**B**) or chromosome-bridged cells (**C**). Each bar represents mean ± SEM of three biological replicates (total of 90 cells per condition). Scale bar, 5 μm. (**D**) Focus formation assay. Representative photo (left) and the number of piled-up colonies (right). Each bar represents mean ± SEM of three biological replicates (total of 90 cells per condition). (**E**) Karyotype analysis of MEFs. Data are mean ± SEM (n = 3, total of 60 cells per condition). (**F**) MEFs were subcutaneously injected into nude mice (n = 6). The weight (left) and photo (right) of tumors after 20 (MEF/MajSAT RNA #2) or 30 (MEF/Vector, MajSAT #1 or MajSAT #3) days. Scale bar, 10 mm. **P* < 0.05, ***P* < 0.01, or ****P* < 0.001 by the unpaired two-sided *t*-test (**B**, **C**, **D**, **E**) or the Kruskal-Wallis *H* test (one-way ANOVA on ranks) and Steel's multiple comparisons post hoc test (**F**).

Figure. S7

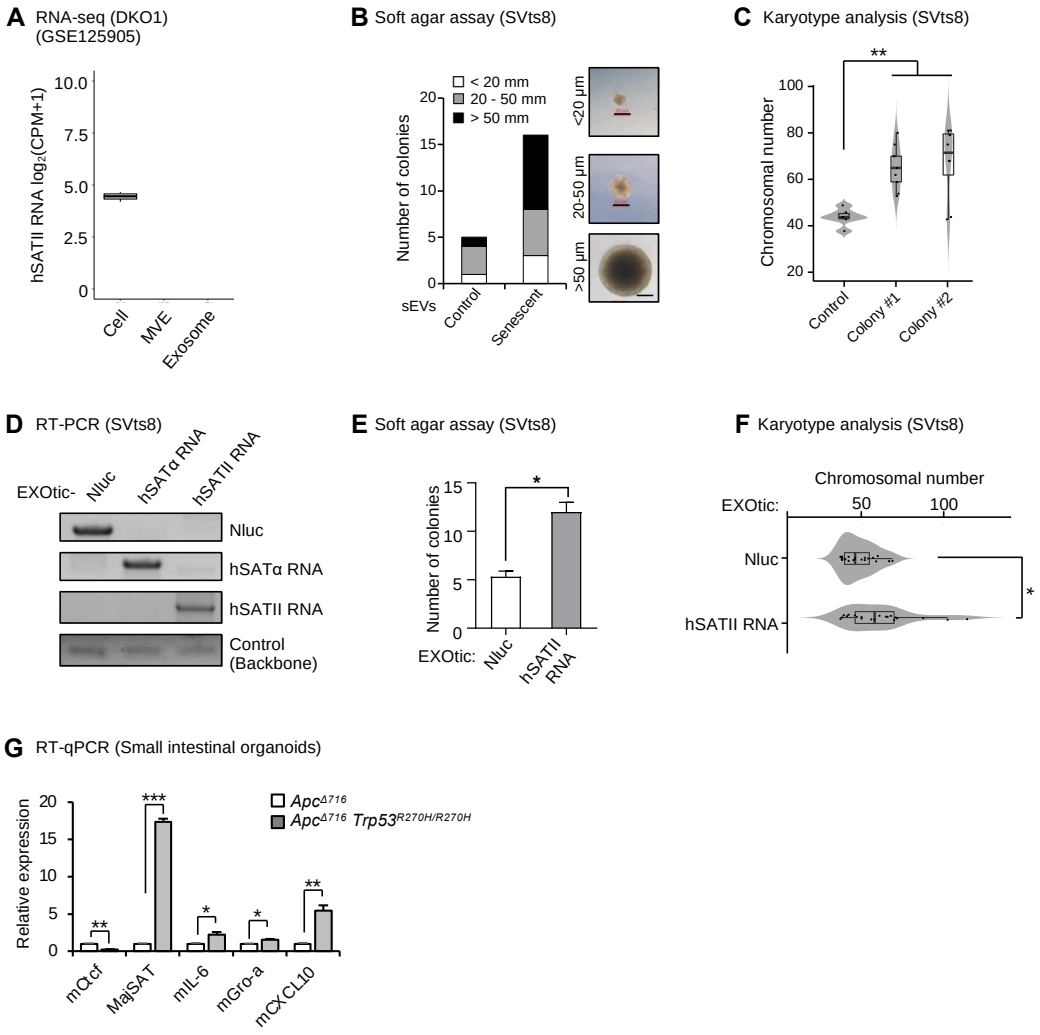

Fig. S7. Pericentromeric satellite RNA in small EVs provokes chromosomal instability.

(**A**) Count per million mapped reads of hSATII RNA detected in cells, multi-vesicular endosome (MVE) or exosomes secreted from cells of human colon cancer cell line, DKO1, (GSE125905) (36). (**B**) Comparison of anchorage-independent growth of SVts8 cells treated with small EVs derived from proliferating or X-ray-induced senescent RPE-1/hTERT cells. The number of colonies was counted (total of 5 independent fields per condition). Scale bar, 20 μm. (**C**) Number of chromosomes in the colonies from *SI Appendix*, Fig. S7*B*, or parent SVts8 cells (n = 8 per condition). (**D**) The incorporation of Nluc, hSATα, or hSATII RNA in designer exosomes produced by the EXOtic devices into SVts8 cells was confirmed by RT-PCR. (**E**) Comparison of anchorage-independent growth of SVts8 cells treated with Nluc (Control) or hSATII RNA-incorporated small EVs by EXOtic devices. The number of colonies was counted (n = 20 per condition). (**F**) The number of chromosomes in the colonies from *SI Appendix*, Fig. S7*E* (n = 20 per condition). (**G**) RT-qPCR analysis of MajSAT, CTCF, and SASP factor genes in a malignant organoid derived from colon cancer ($Apc^{\Delta 716}$ $Trp53^{R270H/R270H}$) compared with its nonmalignant

organoid (*Apc*$^{\Delta 716}$). The relative expression shows the value normalized to that of nonmalignant organoids (*Apc*$^{\Delta 716}$). Each bar represents mean ± SD of three technical replicates repeated in two independent experiments (**G**). In the boxplot, the bottom and top hinges indicate the first and third quartile, respectively. The horizontal lines into the boxes indicate the median. The upper and lower whiskers define the highest and lowest value within 1.5 times of the interquartile range, respectively. **P* < 0.05, ***P* < 0.01, or ****P* < 0.001 by the unpaired two-sided *t*-test (**E**, **F**, **G**) or one-way ANOVA followed by the Dunnett's multiple comparisons post hoc test (**C**).

Table S1. A list of hSATII RNA binding proteins.

Accession	Description	# Unique Peptides
Q9NZB2	Constitutive coactivator of PPAR-gamma-like protein 1 OS=Homo sapiens GN=FAM120A PE=1 SV=2	43
Q08211	ATP-dependent RNA helicase A OS=Homo sapiens GN=DHX9 PE=1 SV=4	42
Q9NR30	Nucleolar RNA helicase 2 OS=Homo sapiens GN=DDX21 PE=1 SV=5	41
Q1KMD3	Heterogeneous nuclear ribonucleoprotein U-like protein 2 OS=Homo sapiens GN=HNRNPUL2 PE=1 SV=1	41
Q12906	Interleukin enhancer-binding factor 3 OS=Homo sapiens GN=ILF3 PE=1 SV=3	37
Q00839	Heterogeneous nuclear ribonucleoprotein U OS=Homo sapiens GN=HNRNPU PE=1 SV=6	35
Q96KR1	Zinc finger RNA-binding protein OS=Homo sapiens GN=ZFR PE=1 SV=2	34
Q9Y6M1	Insulin-like growth factor 2 mRNA-binding protein 2 OS=Homo sapiens GN=IGF2BP2 PE=1 SV=2	31
Q9NZI8	Insulin-like growth factor 2 mRNA-binding protein 1 OS=Homo sapiens GN=IGF2BP1 PE=1 SV=2	28
O43390	Heterogeneous nuclear ribonucleoprotein R OS=Homo sapiens GN=HNRNPR PE=1 SV=1	25
P19338	Nucleolin OS=Homo sapiens GN=NCL PE=1 SV=3	25
O60506	Heterogeneous nuclear ribonucleoprotein Q OS=Homo sapiens GN=SYNCRIP PE=1 SV=2	24
P22626	Heterogeneous nuclear ribonucleoproteins A2/B1 OS=Homo sapiens GN=HNRNPA2B1 PE=1 SV=2	24
P61978	Heterogeneous nuclear ribonucleoprotein K OS=Homo sapiens GN=HNRNPK PE=1 SV=1	23
P49711	**Transcriptional repressor CTCF OS=Homo sapiens GN=CTCF PE=1 SV=1**	22
P04264	Keratin, type II cytoskeletal 1 OS=Homo sapiens GN=KRT1 PE=1 SV=6	19
P51991	Heterogeneous nuclear ribonucleoprotein A3 OS=Homo sapiens GN=HNRNPA3 PE=1 SV=2	19
P14866	Heterogeneous nuclear ribonucleoprotein L OS=Homo sapiens GN=HNRNPL PE=1 SV=2	18
Q5BKZ1	DBIRD complex subunit ZNF326 OS=Homo sapiens GN=ZNF326 PE=1 SV=2	18
P49750	YLP motif-containing protein 1 OS=Homo sapiens GN=YLPM1 PE=1 SV=3	18
P09651	Heterogeneous nuclear ribonucleoprotein A1 OS=Homo sapiens GN=HNRNPA1 PE=1 SV=5	16
Q16630	Heterogeneous nuclear ribonucleoprotein A1 OS=Homo sapiens GN=HNRNPA1 PE=1 SV=5	16
P67809	Nuclease-sensitive element-binding protein 1 OS=Homo sapiens GN=YBX1 PE=1 SV=3	15
P35527	Keratin, type I cytoskeletal 9 OS=Homo sapiens GN=KRT9 PE=1 SV=3	15
Q12905	Interleukin enhancer-binding factor 2 OS=Homo sapiens GN=ILF2 PE=1 SV=2	14
O00571	ATP-dependent RNA helicase DDX3X OS=Homo sapiens GN=DDX3X PE=1 SV=3	14
Q14103	Heterogeneous nuclear ribonucleoprotein D0 OS=Homo sapiens GN=HNRNPD PE=1 SV=1	13
Q7Z2W4	Zinc finger CCCH-type antiviral protein 1 OS=Homo sapiens GN=ZC3HAV1 PE=1 SV=3	13
Q13242	Serine/arginine-rich splicing factor 9 OS=Homo sapiens GN=SRSF9 PE=1 SV=1	13
Q14966	Zinc finger protein 638 OS=Homo sapiens GN=ZNF638 PE=1 SV=2	13
P38159	RNA-binding motif protein, X chromosome OS=Homo sapiens GN=RBMX PE=1 SV=3	12
P31942	Heterogeneous nuclear ribonucleoprotein H3 OS=Homo sapiens GN=HNRNPH3 PE=1 SV=2	12
Q99729	Heterogeneous nuclear ribonucleoprotein A/B OS=Homo sapiens GN=HNRNPAB PE=1 SV=2	12
Q96QR8	Transcriptional activator protein Pur-beta OS=Homo sapiens GN=PURB PE=1 SV=3	12
O00425	Insulin-like growth factor 2 mRNA-binding protein 3 OS=Homo sapiens GN=IGF2BP3 PE=1 SV=2	12
P35908	Keratin, type II cytoskeletal 2 epidermal OS=Homo sapiens GN=KRT2 PE=1 SV=2	12
O76021	Ribosomal L1 domain-containing protein 1 OS=Homo sapiens GN=RSL1D1 PE=1 SV=3	12
P13645	Keratin, type I cytoskeletal 10 OS=Homo sapiens GN=KRT10 PE=1 SV=6	12
P55265	Double-stranded RNA-specific adenosine deaminase OS=Homo sapiens GN=ADAR PE=1 SV=4	12
Q96SI9	Spermatid perinuclear RNA-binding protein OS=Homo sapiens GN=STRBP PE=1 SV=1	11
P17844	Probable ATP-dependent RNA helicase DDX5 OS=Homo sapiens GN=DDX5 PE=1 SV=1	11
P16989	Y-box-binding protein 3 OS=Homo sapiens GN=YBX3 PE=1 SV=4	10
Q07955	Serine/arginine-rich splicing factor 1 OS=Homo sapiens GN=SRSF1 PE=1 SV=2	10
Q9HCD5	Nuclear receptor coactivator 5 OS=Homo sapiens GN=NCOA5 PE=1 SV=2	10
Q15424	Scaffold attachment factor B1 OS=Homo sapiens GN=SAFB PE=1 SV=4	10
Q9BUJ2	Heterogeneous nuclear ribonucleoprotein U-like protein 1 OS=Homo sapiens GN=HNRNPUL1 PE=1 SV=2	10

P46777	60S ribosomal protein L5 OS=Homo sapiens GN=RPL5 PE=1 SV=3	9
P52272	Heterogeneous nuclear ribonucleoprotein M OS=Homo sapiens GN=HNRNPM PE=1 SV=3	9
P18124	60S ribosomal protein L7 OS=Homo sapiens GN=RPL7 PE=1 SV=1	9
P61247	40S ribosomal protein S3a OS=Homo sapiens GN=RPS3A PE=1 SV=2	9
P07910	Heterogeneous nuclear ribonucleoproteins C1/C2 OS=Homo sapiens GN=HNRNPC PE=1 SV=4	9
P31943	Heterogeneous nuclear ribonucleoprotein H OS=Homo sapiens GN=HNRNPH1 PE=1 SV=4	8
P35637	RNA-binding protein FUS OS=Homo sapiens GN=FUS PE=1 SV=1	8
Q00577	Transcriptional activator protein Pur-alpha OS=Homo sapiens GN=PURA PE=1 SV=2	8
O14979	Heterogeneous nuclear ribonucleoprotein D-like OS=Homo sapiens GN=HNRNPDL PE=1 SV=3	8
P11940	Polyadenylate-binding protein 1 OS=Homo sapiens GN=PABPC1 PE=1 SV=2	8
Q9UBU9	Nuclear RNA export factor 1 OS=Homo sapiens GN=NXF1 PE=1 SV=1	8
P36578	60S ribosomal protein L4 OS=Homo sapiens GN=RPL4 PE=1 SV=5	8
O00308	NEDD4-like E3 ubiquitin-protein ligase WWP2 OS=Homo sapiens GN=WWP2 PE=1 SV=2	8
Q99575	Ribonucleases P/MRP protein subunit POP1 OS=Homo sapiens GN=POP1 PE=1 SV=2	8
Q96MU7	YTH domain-containing protein 1 OS=Homo sapiens GN=YTHDC1 PE=1 SV=3	8
P62701	40S ribosomal protein S4, X isoform OS=Homo sapiens GN=RPS4X PE=1 SV=2	8
P39023	60S ribosomal protein L3 OS=Homo sapiens GN=RPL3 PE=1 SV=2	7
Q32P28	Prolyl 3-hydroxylase 1 OS=Homo sapiens GN=P3H1 PE=1 SV=2	7
Q9UHX1	Poly(U)-binding-splicing factor PUF60 OS=Homo sapiens GN=PUF60 PE=1 SV=1	7
Q92804	TATA-binding protein-associated factor 2N OS=Homo sapiens GN=TAF15 PE=1 SV=1	7
Q14151	Scaffold attachment factor B2 OS=Homo sapiens GN=SAFB2 PE=1 SV=1	7
P11142	Heat shock cognate 71 kDa protein OS=Homo sapiens GN=HSPA8 PE=1 SV=1	7
Q12849	G-rich sequence factor 1 OS=Homo sapiens GN=GRSF1 PE=1 SV=3	7
P78406	mRNA export factor OS=Homo sapiens GN=RAE1 PE=1 SV=1	7
Q92841	Probable ATP-dependent RNA helicase DDX17 OS=Homo sapiens GN=DDX17 PE=1 SV=2	7
Q02878	60S ribosomal protein L6 OS=Homo sapiens GN=RPL6 PE=1 SV=3	7
Q13151	Heterogeneous nuclear ribonucleoprotein A0 OS=Homo sapiens GN=HNRNPA0 PE=1 SV=1	6
O43809	Cleavage and polyadenylation specificity factor subunit 5 OS=Homo sapiens GN=NUDT21 PE=1 SV=1	6
Q9H2U1	ATP-dependent RNA helicase DHX36 OS=Homo sapiens GN=DHX36 PE=1 SV=2	6
P62424	60S ribosomal protein L7a OS=Homo sapiens GN=RPL7A PE=1 SV=2	6
P08621	U1 small nuclear ribonucleoprotein 70 kDa OS=Homo sapiens GN=SNRNP70 PE=1 SV=2	6
Q96T58	Msx2-interacting protein OS=Homo sapiens GN=SPEN PE=1 SV=1	6
Q8N684	Cleavage and polyadenylation specificity factor subunit 7 OS=Homo sapiens GN=CPSF7 PE=1 SV=1	6
P05388	60S acidic ribosomal protein P0 OS=Homo sapiens GN=RPLP0 PE=1 SV=1	5
P60709	Actin, cytoplasmic 1 OS=Homo sapiens GN=ACTB PE=1 SV=1	5
P84098	60S ribosomal protein L19 OS=Homo sapiens GN=RPL19 PE=1 SV=1	5
P43243	Matrin-3 OS=Homo sapiens GN=MATR3 PE=1 SV=2	5
P26373	60S ribosomal protein L13 OS=Homo sapiens GN=RPL13 PE=1 SV=4	5
Q9H0D6	5'-3' exoribonuclease 2 OS=Homo sapiens GN=XRN2 PE=1 SV=1	5
O95793	Double-stranded RNA-binding protein Staufen homolog 1 OS=Homo sapiens GN=STAU1 PE=1 SV=2	5
P02768	Serum albumin OS=Homo sapiens GN=ALB PE=1 SV=2	5
P61254	60S ribosomal protein L26 OS=Homo sapiens GN=RPL26 PE=1 SV=1	5
Q15007	Pre-mRNA-splicing regulator WTAP OS=Homo sapiens GN=WTAP PE=1 SV=2	5
P40429	60S ribosomal protein L13a OS=Homo sapiens GN=RPL13A PE=1 SV=2	5
P26368	Splicing factor U2AF 65 kDa subunit OS=Homo sapiens GN=U2AF2 PE=1 SV=4	5
P42285	Superkiller viralicidic activity 2-like 2 OS=Homo sapiens GN=SKIV2L2 PE=1 SV=3	5
Q99590	Protein SCAF11 OS=Homo sapiens GN=SCAF11 PE=1 SV=2	5
P62280	40S ribosomal protein S11 OS=Homo sapiens GN=RPS11 PE=1 SV=3	5
Q9UKM9	RNA-binding protein Raly OS=Homo sapiens GN=RALY PE=1 SV=1	5

Q9UH17	DNA dC->dU-editing enzyme APOBEC-3B OS=Homo sapiens GN=APOBEC3B PE=1 SV=1	5
P09012	U1 small nuclear ribonucleoprotein A OS=Homo sapiens GN=SNRPA PE=1 SV=3	4
Q9UL40	Zinc finger protein 346 OS=Homo sapiens GN=ZNF346 PE=1 SV=1	4
O60832	H/ACA ribonucleoprotein complex subunit 4 OS=Homo sapiens GN=DKC1 PE=1 SV=3	4
Q13310	Polyadenylate-binding protein 4 OS=Homo sapiens GN=PABPC4 PE=1 SV=1	4
P50914	60S ribosomal protein L14 OS=Homo sapiens GN=RPL14 PE=1 SV=4	4
P62913	60S ribosomal protein L11 OS=Homo sapiens GN=RPL11 PE=1 SV=2	4
P02538	Keratin, type II cytoskeletal 6A OS=Homo sapiens GN=KRT6A PE=1 SV=3	4
O95232	Luc7-like protein 3 OS=Homo sapiens GN=LUC7L3 PE=1 SV=2	4
Q86YZ3	Hornerin OS=Homo sapiens GN=HRNR PE=1 SV=2	4
O15504	Nucleoporin-like protein 2 OS=Homo sapiens GN=NUPL2 PE=1 SV=1	4
P62906	60S ribosomal protein L10a OS=Homo sapiens GN=RPL10A PE=1 SV=2	4
Q5T200	Zinc finger CCCH domain-containing protein 13 OS=Homo sapiens GN=ZC3H13 PE=1 SV=1	4
O75683	Surfeit locus protein 6 OS=Homo sapiens GN=SURF6 PE=1 SV=3	4
O75718	Cartilage-associated protein OS=Homo sapiens GN=CRTAP PE=1 SV=1	4
P55795	Heterogeneous nuclear ribonucleoprotein H2 OS=Homo sapiens GN=HNRNPH2 PE=1 SV=1	3
P02533	Keratin, type I cytoskeletal 14 OS=Homo sapiens GN=KRT14 PE=1 SV=4	3
Q13148	TAR DNA-binding protein 43 OS=Homo sapiens GN=TARDBP PE=1 SV=1	3
P25705	ATP synthase subunit alpha, mitochondrial OS=Homo sapiens GN=ATP5A1 PE=1 SV=1	3
Q15717	ELAV-like protein 1 OS=Homo sapiens GN=ELAVL1 PE=1 SV=2	3
O43143	Pre-mRNA-splicing factor ATP-dependent RNA helicase DHX15 OS=Homo sapiens GN=DHX15 PE=1 SV=2	3
Q14498	RNA-binding protein 39 OS=Homo sapiens GN=RBM39 PE=1 SV=2	3
Q9Y383	Putative RNA-binding protein Luc7-like 2 OS=Homo sapiens GN=LUC7L2 PE=1 SV=2	3
P23396	40S ribosomal protein S3 OS=Homo sapiens GN=RPS3 PE=1 SV=2	3
P30050	60S ribosomal protein L12 OS=Homo sapiens GN=RPL12 PE=1 SV=1	3
P62140	Serine/threonine-protein phosphatase PP1-beta catalytic subunit OS=Homo sapiens GN=PPP1CB PE=1 SV=3	3
Q9UDY2	Tight junction protein ZO-2 OS=Homo sapiens GN=TJP2 PE=1 SV=2	3
Q96J02	E3 ubiquitin-protein ligase Itchy homolog OS=Homo sapiens GN=ITCH PE=1 SV=2	3
O60814	Histone H2B type 1-K OS=Homo sapiens GN=HIST1H2BK PE=1 SV=3	3
Q01081	Splicing factor U2AF 35 kDa subunit OS=Homo sapiens GN=U2AF1 PE=1 SV=3	3
Q04837	Single-stranded DNA-binding protein, mitochondrial OS=Homo sapiens GN=SSBP1 PE=1 SV=1	3
P15880	40S ribosomal protein S2 OS=Homo sapiens GN=RPS2 PE=1 SV=2	3
P62753	40S ribosomal protein S6 OS=Homo sapiens GN=RPS6 PE=1 SV=1	3
Q01130	Serine/arginine-rich splicing factor 2 OS=Homo sapiens GN=SRSF2 PE=1 SV=4	3
P23246	Splicing factor, proline- and glutamine-rich OS=Homo sapiens GN=SFPQ PE=1 SV=2	3
Q02543	60S ribosomal protein L18a OS=Homo sapiens GN=RPL18A PE=1 SV=2	3
Q9Y2W1	Thyroid hormone receptor-associated protein 3 OS=Homo sapiens GN=THRAP3 PE=1 SV=2	3
P13647	Keratin, type II cytoskeletal 5 OS=Homo sapiens GN=KRT5 PE=1 SV=3	3
P23284	Peptidyl-prolyl cis-trans isomerase B OS=Homo sapiens GN=PPIB PE=1 SV=2	3
P62318	Small nuclear ribonucleoprotein Sm D3 OS=Homo sapiens GN=SNRPD3 PE=1 SV=1	3
Q9BQ67	Glutamate-rich WD repeat-containing protein 1 OS=Homo sapiens GN=GRWD1 PE=1 SV=1	3
P46779	60S ribosomal protein L28 OS=Homo sapiens GN=RPL28 PE=1 SV=3	3
P98179	RNA-binding protein 3 OS=Homo sapiens GN=RBM3 PE=1 SV=1	3
Q96PM9	Zinc finger protein 385A OS=Homo sapiens GN=ZNF385A PE=1 SV=2	3
Q8NEY8	Periphilin-1 OS=Homo sapiens GN=PPHLN1 PE=1 SV=2	3
Q9Y3Y2	Chromatin target of PRMT1 protein OS=Homo sapiens GN=CHTOP PE=1 SV=2	2
Q4G0J3	La-related protein 7 OS=Homo sapiens GN=LARP7 PE=1 SV=1	2
P62750	60S ribosomal protein L23a OS=Homo sapiens GN=RPL23A PE=1 SV=1	2
P68871	Hemoglobin subunit beta OS=Homo sapiens GN=HBB PE=1 SV=2	2

Q86U42	Polyadenylate-binding protein 2 OS=Homo sapiens GN=PABPN1 PE=1 SV=3	2
P02545	Prelamin-A/C OS=Homo sapiens GN=LMNA PE=1 SV=1	2
Q13610	Periodic tryptophan protein 1 homolog OS=Homo sapiens GN=PWP1 PE=1 SV=1	2
P62316	Small nuclear ribonucleoprotein Sm D2 OS=Homo sapiens GN=SNRPD2 PE=1 SV=1	2
Q16629	Serine/arginine-rich splicing factor 7 OS=Homo sapiens GN=SRSF7 PE=1 SV=1	2
O75533	Splicing factor 3B subunit 1 OS=Homo sapiens GN=SF3B1 PE=1 SV=3	2
Q96SB4	SRSF protein kinase 1 OS=Homo sapiens GN=SRPK1 PE=1 SV=2	2
P11021	78 kDa glucose-regulated protein OS=Homo sapiens GN=HSPA5 PE=1 SV=2	2
Q9Y520	Protein PRRC2C OS=Homo sapiens GN=PRRC2C PE=1 SV=4	2
P06748	Nucleophosmin OS=Homo sapiens GN=NPM1 PE=1 SV=2	2
Q05639	Elongation factor 1-alpha 2 OS=Homo sapiens GN=EEF1A2 PE=1 SV=1	2
Q86VM9	Zinc finger CCCH domain-containing protein 18 OS=Homo sapiens GN=ZC3H18 PE=1 SV=2	2
P08865	40S ribosomal protein SA OS=Homo sapiens GN=RPSA PE=1 SV=4	2
P05412	Transcription factor AP-1 OS=Homo sapiens GN=JUN PE=1 SV=2	2
Q13243	Serine/arginine-rich splicing factor 5 OS=Homo sapiens GN=SRSF5 PE=1 SV=1	2
P46781	40S ribosomal protein S9 OS=Homo sapiens GN=RPS9 PE=1 SV=3	2
Q15365	Poly(rC)-binding protein 1 OS=Homo sapiens GN=PCBP1 PE=1 SV=2	2
P08708	40S ribosomal protein S17 OS=Homo sapiens GN=RPS17 PE=1 SV=2	2
P39019	40S ribosomal protein S19 OS=Homo sapiens GN=RPS19 PE=1 SV=2	2
Q7L2E3	Putative ATP-dependent RNA helicase DHX30 OS=Homo sapiens GN=DHX30 PE=1 SV=1	2
Q00059	Transcription factor A, mitochondrial OS=Homo sapiens GN=TFAM PE=1 SV=1	2
P51114	Fragile X mental retardation syndrome-related protein 1 OS=Homo sapiens GN=FXR1 PE=1 SV=3	2
P18621	60S ribosomal protein L17 OS=Homo sapiens GN=RPL17 PE=1 SV=3	2
O15015	Zinc finger protein 646 OS=Homo sapiens GN=ZNF646 PE=1 SV=1	2
Q15393	Splicing factor 3B subunit 3 OS=Homo sapiens GN=SF3B3 PE=1 SV=4	2
Q15029	116 kDa U5 small nuclear ribonucleoprotein component OS=Homo sapiens GN=EFTUD2 PE=1 SV=1	2
Q12874	Splicing factor 3A subunit 3 OS=Homo sapiens GN=SF3A3 PE=1 SV=1	2
Q15233	Non-POU domain-containing octamer-binding protein OS=Homo sapiens GN=NONO PE=1 SV=4	2
Q9H5H4	Zinc finger protein 768 OS=Homo sapiens GN=ZNF768 PE=1 SV=2	2
Q15149	Plectin OS=Homo sapiens GN=PLEC PE=1 SV=3	2
P30876	DNA-directed RNA polymerase II subunit RPB2 OS=Homo sapiens GN=POLR2B PE=1 SV=1	2
P20700	Lamin-B1 OS=Homo sapiens GN=LMNB1 PE=1 SV=2	2
P62081	40S ribosomal protein S7 OS=Homo sapiens GN=RPS7 PE=1 SV=1	2
P12956	X-ray repair cross-complementing protein 6 OS=Homo sapiens GN=XRCC6 PE=1 SV=2	2
Q96Q89	Kinesin-like protein KIF20B OS=Homo sapiens GN=KIF20B PE=1 SV=3	1
P62910	60S ribosomal protein L32 OS=Homo sapiens GN=RPL32 PE=1 SV=2	1
Q9NY46	Sodium channel protein type 3 subunit alpha OS=Homo sapiens GN=SCN3A PE=1 SV=2	1
P46782	40S ribosomal protein S5 OS=Homo sapiens GN=RPS5 PE=1 SV=4	1
P81605	Dermcidin OS=Homo sapiens GN=DCD PE=1 SV=2	1
P05164	Myeloperoxidase OS=Homo sapiens GN=MPO PE=1 SV=1	1
P18077	60S ribosomal protein L35a OS=Homo sapiens GN=RPL35A PE=1 SV=2	1
Q5SZL2	Centrosomal protein of 85 kDa-like OS=Homo sapiens GN=CEP85L PE=1 SV=1	1
P49790	Nuclear pore complex protein Nup153 OS=Homo sapiens GN=NUP153 PE=1 SV=2	1
P62891	60S ribosomal protein L39 OS=Homo sapiens GN=RPL39 PE=1 SV=2	1
Q9Y4K1	Beta/gamma crystallin domain-containing protein 1 OS=Homo sapiens GN=CRYBG1 PE=1 SV=3	1
O75808	Calpain-15 OS=Homo sapiens GN=CAPN15 PE=1 SV=1	1
Q17RY0	Cytoplasmic polyadenylation element-binding protein 4 OS=Homo sapiens GN=CPEB4 PE=1 SV=1	1
Q92800	Histone-lysine N-methyltransferase EZH1 OS=Homo sapiens GN=EZH1 PE=1 SV=2	1
Q92673	Sortilin-related receptor OS=Homo sapiens GN=SORL1 PE=1 SV=2	1

Q96E39	RNA binding motif protein, X-linked-like-1 OS=Homo sapiens GN=RBMXL1 PE=1 SV=1	1
P48735	Isocitrate dehydrogenase [NADP], mitochondrial OS=Homo sapiens GN=IDH2 PE=1 SV=2	1
Q5SSJ5	Heterochromatin protein 1-binding protein 3 OS=Homo sapiens GN=HP1BP3 PE=1 SV=1	1
P84103	Serine/arginine-rich splicing factor 3 OS=Homo sapiens GN=SRSF3 PE=1 SV=1	1
P52597	Heterogeneous nuclear ribonucleoprotein F OS=Homo sapiens GN=HNRNPF PE=1 SV=3	1
P82650	28S ribosomal protein S22, mitochondrial OS=Homo sapiens GN=MRPS22 PE=1 SV=1	1
P62241	40S ribosomal protein S8 OS=Homo sapiens GN=RPS8 PE=1 SV=2	1
P62277	40S ribosomal protein S13 OS=Homo sapiens GN=RPS13 PE=1 SV=2	1
P51116	Fragile X mental retardation syndrome-related protein 2 OS=Homo sapiens GN=FXR2 PE=1 SV=2	1
P52292	Importin subunit alpha-1 OS=Homo sapiens GN=KPNA2 PE=1 SV=1	1
P62917	60S ribosomal protein L8 OS=Homo sapiens GN=RPL8 PE=1 SV=2	1
P35268	60S ribosomal protein L22 OS=Homo sapiens GN=RPL22 PE=1 SV=2	1
P47914	60S ribosomal protein L29 OS=Homo sapiens GN=RPL29 PE=1 SV=2	1
P11387	DNA topoisomerase 1 OS=Homo sapiens GN=TOP1 PE=1 SV=2	1
P13010	X-ray repair cross-complementing protein 5 OS=Homo sapiens GN=XRCC5 PE=1 SV=3	1
Q9BXP5	Serrate RNA effector molecule homolog OS=Homo sapiens GN=SRRT PE=1 SV=1	1
P78362	SRSF protein kinase 2 OS=Homo sapiens GN=SRPK2 PE=1 SV=3	1
P17535	Transcription factor jun-D OS=Homo sapiens GN=JUND PE=1 SV=3	1
Q13838	Spliceosome RNA helicase DDX39B OS=Homo sapiens GN=DDX39B PE=1 SV=1	1
P61313	60S ribosomal protein L15 OS=Homo sapiens GN=RPL15 PE=1 SV=2	1
P21399	Cytoplasmic aconitate hydratase OS=Homo sapiens GN=ACO1 PE=1 SV=3	1
P69905	Hemoglobin subunit alpha OS=Homo sapiens GN=HBA1 PE=1 SV=2	1
Q07020	60S ribosomal protein L18 OS=Homo sapiens GN=RPL18 PE=1 SV=2	1
P31327	Carbamoyl-phosphate synthase [ammonia], mitochondrial OS=Homo sapiens GN=CPS1 PE=1 SV=2	1
P23526	Adenosylhomocysteinase OS=Homo sapiens GN=AHCY PE=1 SV=4	1
P16104	Histone H2AX OS=Homo sapiens GN=H2AFX PE=1 SV=2	1
Q13573	SNW domain-containing protein 1 OS=Homo sapiens GN=SNW1 PE=1 SV=1	1
Q9UPT8	Zinc finger CCCH domain-containing protein 4 OS=Homo sapiens GN=ZC3H4 PE=1 SV=3	1
Q96T37	Putative RNA-binding protein 15 OS=Homo sapiens GN=RBM15 PE=1 SV=2	1
Q9BZF9	Uveal autoantigen with coiled-coil domains and ankyrin repeats OS=Homo sapiens GN=UACA PE=1 SV=2	1
Q8NAF0	Zinc finger protein 579 OS=Homo sapiens GN=ZNF579 PE=1 SV=2	1
Q49A26	Putative oxidoreductase GLYR1 OS=Homo sapiens GN=GLYR1 PE=1 SV=3	1
P08579	U2 small nuclear ribonucleoprotein B" OS=Homo sapiens GN=SNRPB2 PE=1 SV=1	1
P06576	ATP synthase subunit beta, mitochondrial OS=Homo sapiens GN=ATP5B PE=1 SV=3	1
Q96NZ9	Proline-rich acidic protein 1 OS=Homo sapiens GN=PRAP1 PE=1 SV=2	1
P82930	28S ribosomal protein S34, mitochondrial OS=Homo sapiens GN=MRPS34 PE=1 SV=2	1
Q9BRU9	rRNA-processing protein UTP23 homolog OS=Homo sapiens GN=UTP23 PE=1 SV=2	1
Q9NWH9	SAFB-like transcription modulator OS=Homo sapiens GN=SLTM PE=1 SV=2	1
Q03252	Lamin-B2 OS=Homo sapiens GN=LMNB2 PE=1 SV=4	1
P62263	40S ribosomal protein S14 OS=Homo sapiens GN=RPS14 PE=1 SV=3	1
P14678	Small nuclear ribonucleoprotein-associated proteins B and B' OS=Homo sapiens GN=SNRPB PE=1 SV=2	1
Q15434	RNA-binding motif, single-stranded-interacting protein 2 OS=Homo sapiens GN=RBMS2 PE=1 SV=1	1
Q7Z6E9	E3 ubiquitin-protein ligase RBBP6 OS=Homo sapiens GN=RBBP6 PE=1 SV=1	1
Q9Y580	RNA-binding protein 7 OS=Homo sapiens GN=RBM7 PE=1 SV=1	1
P49207	60S ribosomal protein L34 OS=Homo sapiens GN=RPL34 PE=1 SV=3	1
Q66PJ3	ADP-ribosylation factor-like protein 6-interacting protein 4 OS=Homo sapiens GN=ARL6IP4 PE=1 SV=2	1
Q9NRW3	DNA dC->dU-editing enzyme APOBEC-3C OS=Homo sapiens GN=APOBEC3C PE=1 SV=2	1
Q8TBF4	Zinc finger CCHC-type and RNA-binding motif-containing protein 1 OS=Homo sapiens GN=ZCRB1 PE=1 SV=2	1
Q8NEF9	Serum response factor-binding protein 1 OS=Homo sapiens GN=SRFBP1 PE=1 SV=1	1

P08670	Vimentin OS=Homo sapiens GN=VIM PE=1 SV=4	1
O00746	Nucleoside diphosphate kinase, mitochondrial OS=Homo sapiens GN=NME4 PE=1 SV=1	1
P02751	Fibronectin OS=Homo sapiens GN=FN1 PE=1 SV=4	1
Q9UMS4	Pre-mRNA-processing factor 19 OS=Homo sapiens GN=PRPF19 PE=1 SV=1	1
Q15459	Splicing factor 3A subunit 1 OS=Homo sapiens GN=SF3A1 PE=1 SV=1	1
Q5VWQ0	Round spermatid basic protein 1 OS=Homo sapiens GN=RSBN1 PE=1 SV=2	1
Q9BWU0	Kanadaptin OS=Homo sapiens GN=SLC4A1AP PE=1 SV=1	1
O95639	Cleavage and polyadenylation specificity factor subunit 4 OS=Homo sapiens GN=CPSF4 PE=1 SV=1	1
Q6NZY4	Zinc finger CCHC domain-containing protein 8 OS=Homo sapiens GN=ZCCHC8 PE=1 SV=2	1
P04406	Glyceraldehyde-3-phosphate dehydrogenase OS=Homo sapiens GN=GAPDH PE=1 SV=3	1
Q6NSZ9	Zinc finger and SCAN domain-containing protein 25 OS=Homo sapiens GN=ZSCAN25 PE=1 SV=3	1
Q14011	Cold-inducible RNA-binding protein OS=Homo sapiens GN=CIRBP PE=1 SV=1	1
Q6XE24	RNA-binding motif, single-stranded-interacting protein 3 OS=Homo sapiens GN=RBMS3 PE=1 SV=1	1
P62304	Small nuclear ribonucleoprotein E OS=Homo sapiens GN=SNRPE PE=1 SV=1	1
P42766	60S ribosomal protein L35 OS=Homo sapiens GN=RPL35 PE=1 SV=2	1
Q9NPE3	H/ACA ribonucleoprotein complex subunit 3 OS=Homo sapiens GN=NOP10 PE=1 SV=1	1
Q92794	Histone acetyltransferase KAT6A OS=Homo sapiens GN=KAT6A PE=1 SV=2	1
Q14692	Ribosome biogenesis protein BMS1 homolog OS=Homo sapiens GN=BMS1 PE=1 SV=1	1
Q14683	Structural maintenance of chromosomes protein 1A OS=Homo sapiens GN=SMC1A PE=1 SV=2	1
Q9NQ29	Putative RNA-binding protein Luc7-like 1 OS=Homo sapiens GN=LUC7L PE=1 SV=1	1
P17020	Zinc finger protein 16 OS=Homo sapiens GN=ZNF16 PE=1 SV=3	1
P56537	Eukaryotic translation initiation factor 6 OS=Homo sapiens GN=EIF6 PE=1 SV=1	1
Q13595	Transformer-2 protein homolog alpha OS=Homo sapiens GN=TRA2A PE=1 SV=1	1
A6NKH3	Putative 60S ribosomal protein L37a-like protein OS=Homo sapiens GN=RPL37AP8 PE=5 SV=2	1
P62266	40S ribosomal protein S23 OS=Homo sapiens GN=RPS23 PE=1 SV=3	1
P39656	Dolichyl-diphosphooligosaccharide--protein glycosyltransferase 48 kDa subunit OS=Homo sapiens GN=DDOST PE=1 SV=4	1
O43148	mRNA cap guanine-N7 methyltransferase OS=Homo sapiens GN=RNMT PE=1 SV=1	1
O75665	Oral-facial-digital syndrome 1 protein OS=Homo sapiens GN=OFD1 PE=1 SV=1	1
P78332	RNA-binding protein 6 OS=Homo sapiens GN=RBM6 PE=1 SV=5	1
Q06124	Tyrosine-protein phosphatase non-receptor type 11 OS=Homo sapiens GN=PTPN11 PE=1 SV=2	1
Q10570	Cleavage and polyadenylation specificity factor subunit 1 OS=Homo sapiens GN=CPSF1 PE=1 SV=2	1
Q13435	Splicing factor 3B subunit 2 OS=Homo sapiens GN=SF3B2 PE=1 SV=2	1
Q9NUL3	Double-stranded RNA-binding protein Staufen homolog 2 OS=Homo sapiens GN=STAU2 PE=1 SV=1	1
P01782	Immunoglobulin heavy variable 3-9 OS=Homo sapiens GN=IGHV3-9 PE=1 SV=2	1
P61353	60S ribosomal protein L27 OS=Homo sapiens GN=RPL27 PE=1 SV=2	1
Q8IXT5	RNA-binding protein 12B OS=Homo sapiens GN=RBM12B PE=1 SV=2	1
P05165	Propionyl-CoA carboxylase alpha chain, mitochondrial OS=Homo sapiens GN=PCCA PE=1 SV=4	1
P62888	60S ribosomal protein L30 OS=Homo sapiens GN=RPL30 PE=1 SV=2	1

SI References

1. A. Takahashi *et al.*, DNA damage signaling triggers degradation of histone methyltransferases through APC/C(Cdh1) in senescent cells. *Mol Cell* **45**, 123-131 (2012).
2. A. Takahashi *et al.*, Downregulation of cytoplasmic DNases is implicated in cytoplasmic DNA accumulation and SASP in senescent cells. *Nat Commun* **9**, 1249 (2018).
3. A. Takahashi *et al.*, Exosomes maintain cellular homeostasis by excreting harmful DNA from cells. *Nat Commun* **8**, 15287 (2017).
4. M. Takasugi *et al.*, Small extracellular vesicles secreted from senescent cells promote cancer cell proliferation through EphA2. *Nat Commun* **8**, 15729 (2017).
5. A. Takahashi *et al.*, Mitogenic signalling and the p16INK4a-Rb pathway cooperate to enforce irreversible cellular senescence. *Nat Cell Biol* **8**, 1291-1297 (2006).
6. S. Takeuchi *et al.*, Intrinsic cooperation between p16INK4a and p21Waf1/Cip1 in the onset of cellular senescence and tumor suppression in vivo. *Cancer Res* **70**, 9381-9390 (2010).
7. G. J. Hannon *et al.*, MaRX: an approach to genetics in mammalian cells. *Science* **283**, 1129-1130 (1999).
8. R. Saldana-Meyer *et al.*, RNA Interactions Are Essential for CTCF-Mediated Genome Organization. *Mol Cell* **76**, 412-422 e415 (2019).
9. A. Freund, R. M. Laberge, M. Demaria, J. Campisi, Lamin B1 loss is a senescence-associated biomarker. *Mol Biol Cell* **23**, 2066-2075 (2012).
10. Z. Deng *et al.*, A role for CTCF and cohesin in subtelomere chromatin organization, TERRA transcription, and telomere end protection. *EMBO J* **31**, 4165-4178 (2012).
11. C. M. Azzalin, P. Reichenbach, L. Khoriauli, E. Giulotto, J. Lingner, Telomeric repeat containing RNA and RNA surveillance factors at mammalian chromosome ends. *Science* **318**, 798-801 (2007).
12. Y. Zhou *et al.*, Metascape provides a biologist-oriented resource for the analysis of systems-level datasets. *Nat Commun* **10**, 1523 (2019).
13. K. S. Wendt *et al.*, Cohesin mediates transcriptional insulation by CCCTC-binding factor. *Nature* **451**, 796-801 (2008).
14. J. T. Kung *et al.*, Locus-specific targeting to the X chromosome revealed by the RNA interactome of CTCF. *Mol Cell* **57**, 361-375 (2015).
15. H. Hagege *et al.*, Quantitative analysis of chromosome conformation capture assays (3C-qPCR). *Nat Protoc* **2**, 1722-1733 (2007).
16. M. R. Corces *et al.*, An improved ATAC-seq protocol reduces background and enables interrogation of frozen tissues. *Nat Methods* **14**, 959-962 (2017).
17. T. Mishiro *et al.*, Architectural roles of multiple chromatin insulators at the human apolipoprotein gene cluster. *EMBO J* **28**, 1234-1245 (2009).
18. T. Hirota, D. Gerlich, B. Koch, J. Ellenberg, J. M. Peters, Distinct functions of condensin I and II in mitotic chromosome assembly. *J Cell Sci* **117**, 6435-6445 (2004).

19. R. Kojima *et al.*, Designer exosomes produced by implanted cells intracerebrally deliver therapeutic cargo for Parkinson's disease treatment. *Nat Commun* **9**, 1305 (2018).
20. M. Nakayama *et al.*, Intestinal cancer progression by mutant p53 through the acquisition of invasiveness associated with complex glandular formation. *Oncogene* **36**, 5885-5896 (2017).
21. B. Langmead, S. L. Salzberg, Fast gapped-read alignment with Bowtie 2. *Nat Methods* **9**, 357-359 (2012).
22. H. Li, A statistical framework for SNP calling, mutation discovery, association mapping and population genetical parameter estimation from sequencing data. *Bioinformatics* **27**, 2987-2993 (2011).
23. H. Li *et al.*, The Sequence Alignment/Map format and SAMtools. *Bioinformatics* **25**, 2078-2079 (2009).
24. Y. Zhang *et al.*, Model-based analysis of ChIP-Seq (MACS). *Genome Biol* **9**, R137 (2008).
25. H. Shin, T. Liu, A. K. Manrai, X. S. Liu, CEAS: cis-regulatory element annotation system. *Bioinformatics* **25**, 2605-2606 (2009).
26. A. R. Quinlan, I. M. Hall, BEDTools: a flexible suite of utilities for comparing genomic features. *Bioinformatics* **26**, 841-842 (2010).
27. G. Casella *et al.*, Transcriptome signature of cellular senescence. *Nucleic Acids Res* **47**, 7294-7305 (2019).
28. D. Kim, B. Langmead, S. L. Salzberg, HISAT: a fast spliced aligner with low memory requirements. *Nat Methods* **12**, 357-360 (2015).
29. Y. Liao, G. K. Smyth, W. Shi, featureCounts: an efficient general purpose program for assigning sequence reads to genomic features. *Bioinformatics* **30**, 923-930 (2014).
30. S. W. Criscione, Y. Zhang, W. Thompson, J. M. Sedivy, N. Neretti, Transcriptional landscape of repetitive elements in normal and cancer human cells. *BMC Genomics* **15**, 583 (2014).
31. M. D. Robinson, D. J. McCarthy, G. K. Smyth, edgeR: a Bioconductor package for differential expression analysis of digital gene expression data. *Bioinformatics* **26**, 139-140 (2010).
32. J. T. Robinson *et al.*, Integrative genomics viewer. *Nat Biotechnol* **29**, 24-26 (2011).
33. H. Thorvaldsdottir, J. T. Robinson, J. P. Mesirov, Integrative Genomics Viewer (IGV): high-performance genomics data visualization and exploration. *Brief Bioinform* **14**, 178-192 (2013).
34. M. Pertea *et al.*, StringTie enables improved reconstruction of a transcriptome from RNA-seq reads. *Nat Biotechnol* **33**, 290-295 (2015).
35. A. Subramanian *et al.*, Gene set enrichment analysis: a knowledge-based approach for interpreting genome-wide expression profiles. *Proc Natl Acad Sci U S A* **102**, 15545-15550 (2005).
36. D. K. Jeppesen *et al.*, Reassessment of Exosome Composition. *Cell* **177**, 428-445 e418 (2019).

37. F. Ramirez, F. Dundar, S. Diehl, B. A. Gruning, T. Manke, deepTools: a flexible platform for exploring deep-sequencing data. *Nucleic Acids Res* **42**, W187-191 (2014).
38. S. S. Rao *et al.*, A 3D map of the human genome at kilobase resolution reveals principles of chromatin looping. *Cell* **159**, 1665-1680 (2014).
39. Y. Wang *et al.*, The 3D Genome Browser: a web-based browser for visualizing 3D genome organization and long-range chromatin interactions. *Genome Biol* **19**, 151 (2018).